Journal of Manufacturing and Materials Processing

MDPI

Article

Optimizing the Mechanical Performance of 3D-Printed PLA, ABS, and PETG Through Infill Density and Pattern

Antonio López-Uceda *, Rocío Ruiz-Bustos, Joost Van Duijn and María Isabel López-Martínez

Department of Mechanics, Materials Science and Metallurgical Engineering Area, School of Engineering Sciences, University of Córdoba, University Campus of Rabanales, Leonardo da Vinci Building, Ctra. Nal. IV, km 396, 14071 Córdoba, Spain; rrbustos@uco.es (R.R.-B.); me2vavaj@uco.es (J.V.D.); q12lomam@uco.es (M.I.L.-M.)

* Correspondence: p62louca@uco.es

Abstract

This study investigates the influence of infill density and pattern on the mechanical properties of 3D-printed specimens produced with the most commonly used filaments, such as PLA, ABS, and PETG. A total of 810 standardized samples were fabricated and tested in compression, flexure, and tension, covering six rectilinear infill patterns (Lines, Grid, Triangles, Tri-Hexagon, Cubic, and Octet) at three densities (20, 60, and 100%). One-way ANOVA and Hsu's Multiple Comparisons with the Best were used to compare performance. Strength generally increased with infill density, with the highest values obtained at 100%. PLA exhibited the highest mean compressive, flexural, and tensile strengths, 51.76, 68.03, and 36.60 MPa, respectively, exceeding ABS and PETG by approximately 59–61%, 46–51%, and 73–97%. PETG exhibited the highest mean strain at compressive strength (0.087), compared with 0.061 for PLA and 0.063 for ABS. No single infill pattern performed best across all conditions. Tri-Hexagon achieved the highest or statistically equivalent flexural strength for PLA and PETG at all tested densities, whereas Grid performed best for ABS at 20–60% infill. The 54 linear regressions described strength–density relationships, with R^2 values ranging from approximately 0.70 to 1.00; 44 models yielded $R^2 \geq 0.859$. Intermediate-density estimates and pattern crossover points are conditional on the assumed linear relationships. The framework provides preliminary guidance for selecting infill configurations for specified strength requirements within the investigated materials and processing conditions.

Keywords: fused filament fabrication; commercial filaments; mechanical testing; Hsu's Multiple Comparisons with the Best; infill optimization

Academic Editor: Joshua M. Pearce

Received: 20 October 2026
Revised: 23 November 2026
Accepted: 24 November 2026
Published: 26 November 2026

Copyright: © 2026 by the authors. Licensee MDPI, Basel, Switzerland. This article is an open access article distributed under the terms and conditions of the Creative Commons Attribution (CC BY) license.

1. Introduction

Additive manufacturing (AM), commonly known as 3D printing, is increasingly being adopted in the aerospace, automotive, healthcare, and consumer industries because it enables the fabrication of complex geometries, reduces material waste, and supports rapid prototyping. Among AM techniques, fused filament fabrication (FFF) is widely used. In this process, the infill density, infill pattern, and material type strongly influence the mechanical behaviour of printed parts.

Among thermoplastics used in FFF, polylactic acid (PLA) and acrylonitrile butadiene styrene (ABS) are the most commonly employed, followed closely by polyethylene

terephthalate glycol-modified (PETG) [1,2]. PLA is a biodegradable polymer with high stiffness but low toughness. ABS offers greater impact resistance and thermal stability but is more prone to warping, whereas PETG provides a balance of strength and chemical resistance [3,4]. Their contrasting behaviours make them suitable for comparative evaluation.

Several studies have explored how infill density and pattern influence the mechanical properties of 3D-printed parts. Riza et al. [5] found that increasing the infill density in PLA and ABS improves tensile strength and hardness, with PLA outperforming ABS at all densities tested. Keat et al. [6] observed a strong correlation between infill density and ultimate tensile strength in pure PLA. Agrawal et al. [7] investigated the combined effects of pattern, infill density, and layer thickness on the tensile and impact properties of FFF-printed ABS specimens. Within the investigated conditions, the concentric pattern at 80% infill density and a layer thickness of 0.1 mm provided the highest tensile and impact strengths. Kadhum et al. [8] compared 14 infill patterns using PLA, PLA+ (PLA enhanced by carbon nanoparticles), and PETG, identifying cubic, gyroid, and concentric as the best-performing patterns for each material, respectively. Similarly, Ortega et al. [9] demonstrated that both infill pattern and density significantly affect the strength of PLA samples, particularly under tensile loads. Srinivasan et al. [10] examined the influence of infill density on the tensile properties of PETG parts produced via FDM, reporting a clear positive correlation between density and ultimate tensile strength. Their findings highlight the sensitivity of PETG's mechanical response to internal structure, underscoring the need to include this material in comparative analyses with PLA and ABS.

Other investigations have examined additional process parameters that indirectly influence performance. Hebda et al. [11] analyzed deposition geometry in PLA and ABS as a function of nozzle gap height, extrusion speed, and bed temperature, demonstrating their role in inter-layer bonding. Erdas et al. [12] and Kopar and Yildiz [13] studied the effect of printing angles on PLA, ABS, and PETG parts at 100% infill, reporting PLA as the top performer in compression, bending, and tension, while PETG provides greater strain tolerance. Gao et al. [14] conducted a systematic review on FFF produced with PLA, ABS, and PETG filaments, among others, examining the influence of process parameters such as infill density, build orientation, and printing temperature on tensile, flexural, and impact strength. Their results confirmed that both material type and internal structure have a significant effect on mechanical performance, supporting the need for systematic multi-material investigations such as the one presented in this work.

Recent work by Xu et al. [15] developed data-driven models to predict the flexural performance of PLA–ABS parts as a function of infill parameters, demonstrating the value of predictive approaches for optimizing FFF components. Braconnier et al. [16] applied a design of experiments and principal component analysis to identify the most influential FFF parameters affecting the mechanical performance of ABS, highlighting extrusion temperature and layer thickness as the key factors.

Recent studies have extended the investigation of infill parameters to comparative assessments of commonly used thermoplastics. Menargues et al. [17] examined the effects of processing parameters, including infill pattern and density, on the tensile performance of PLA, ABS, and PETG using 495 specimens. Their findings demonstrated that tensile strength depends on both material selection and processing conditions. Similarly, Kutsal et al. [18] investigated the tensile properties of these three polymers using linear, triangular, and honeycomb patterns at infill densities of 15%, 30%, and 45%. Their ANOVA results identified material type as the main contributor to the variation in tensile strength within the investigated experimental domain. These studies provide valuable comparative evidence across materials; however, their focus on tensile loading leaves open the

question of whether the relative performance of infill configurations is maintained under flexural and compressive loading.

The importance of loading conditions and deposition orientation is illustrated by Buss et al. [19], who investigated the flexural performance of FFF-printed PLA with cubic and triangular infill patterns, five infill densities, and three build orientations. By also considering printing time, they demonstrated that selecting an infill configuration requires balancing mechanical performance and manufacturing efficiency. Their results further indicate that conclusions regarding a preferred pattern must be interpreted in relation to density. Nevertheless, their investigation was restricted to PLA and flexural loading, leaving the transferability of these findings to other polymers and loading modes unresolved.

Beyond comparisons of mechanical strength, Shehbaz and Peng [20] evaluated six infill patterns at three density levels in PLA components, considering tensile performance alongside printing time, material consumption, and energy usage. They related differences in performance to the continuity and alignment of deposited filament paths, emphasizing the role of infill architecture in load transfer. This approach demonstrates that the practical value of infill selection extends beyond maximizing strength through increased density. It also highlights the need to distinguish between selecting a configuration for a specified mechanical requirement and performing a multi-objective optimization that explicitly includes manufacturing resources.

Taken together, these studies demonstrate that the mechanical performance of FFF-printed components depends on material, infill architecture, density, and processing conditions. However, the studies discussed above provide complementary evidence within different experimental domains, leaving a need for an integrated assessment of how infill-pattern rankings change across materials, densities, and loading modes. Such a comparison is necessary to establish whether a pattern that performs favourably under one condition retains its advantage under other conditions and to support infill selection for specified mechanical requirements.

The present study addresses this need through a systematic experimental program comprising 810 standardized specimens made from PLA, ABS, and PETG. Six infill patterns (Lines, Grid, Triangles, Tri-Hexagon, Cubic, and Octet) and three infill densities (20%, 60%, and 100%) were evaluated under compression, flexure, and tension. The contribution of this work lies in the integrated assessment of condition-dependent infill-pattern performance across these three materials and loading modes. One-way ANOVA followed by Hsu's Multiple Comparisons with the Best (MCB) was used to identify the best-performing patterns and those not statistically distinguishable from the best within each condition. Linear regression models were also developed to estimate the infill density required to achieve a specified strength and to explore changes in the predicted best-performing pattern with density. These estimates provide guidance for infill selection within the investigated experimental domain, subject to the limitations of the fitted models.

2. Materials and Methods

2.1. Materials

The materials used for 3D printing were PLA Silver Metallic SMARTFIL® (Smart Materials 3D Printing, S.L.U., Alcalá la Real, Spain), ABS SMARTFIL®, and PETG SMARTFIL®. Specimens were designed according to the corresponding standards using SOLIDWORKS 2022 (Dassault Systèmes SolidWorks Corp., Waltham, MA, USA) and exported as STL files, sliced in Ultimaker Cura 4.13.1, and printed on an Ultimaker 2+ Connect (Ultimaker B.V., Geldermalsen, The Netherlands) printer. A 2.85 mm filament diameter was used. Three infill densities (20%, 60% and 100%) and six patterns (Lines, Grid, Triangles, Tri-Hexagon, Cubic, and Octet), all of them rectilinear and polygonal, were selected in Ultimaker Cura software at their default selection.

For PLA filament printing, the process parameters were fixed as follows: layer height: 0.2 mm; wall thickness: 0.8 mm; wall line count: 2; top thickness: 0.75 mm; bottom thickness: 0.75 mm; top layers: 4; bottom layers: 4; printing temperature: 210 °C; print bed temperature: 60 °C; printing speed: 60 mm/s; and layer cooling fan speed: 100%. These printing parameters were taken from the default PLA profile in Ultimaker Cura software. The nozzle was 0.4 mm in diameter and made of brass.

For ABS and PETG, the default material profiles in Ultimaker Cura were used as starting points. Preliminary printing trials were conducted to assess printing behaviour and adjust the processing parameters for each material. These trials indicated that an enclosure was needed under the investigated printing conditions to reduce thermal gradients and warping. The temperature inside the enclosure did not exceed 45 °C. Additionally, an anti-warping adhesive spray was applied to improve build plate adhesion.

The ABS printing settings that differed from those used for PLA were a printing temperature of 250 °C, a build plate temperature of 85 °C, an infill printing speed of 45 mm/s, and a cooling fan speed of 50%. For PETG, the corresponding settings were a printing temperature of 245 °C, a build plate temperature of 85 °C, a printing speed of 40 mm/s, and a cooling fan speed of 20%. All other settings were the same as those used for PLA. The final settings were kept constant for all specimens of each material, while infill pattern and density were varied according to the experimental design. Since material-specific printing parameters were used, the differences among PLA, ABS, and PETG reflect both material characteristics and processing conditions, whose individual contributions cannot be separated within the present experimental design. Consequently, the comparative results apply to the filament grades and printing conditions investigated and should not be generalized to other processing configurations.

Table 1 summarizes the investigated factors and their corresponding levels.

Table 1. Summary of the experimental factors and testing program.

Factor	Levels	Number of Levels
Filament Material	PLA, ABS, PETG	3
Infill pattern	Lines, Grid, Triangles, Tri-Hexagon, Cubic, Octet	6
Infill density	20%, 60%, 100%	3
Mechanical tests	Compression, flexural, tensile	3

2.2. Methods

Compression, flexural and tensile tests were conducted according to UNE-EN ISO 604:2003 [21], UNE-EN ISO 178:2020 [22] and UNE ISO 527-1:2019 [23], respectively. Five specimens were manufactured for each combination of material, infill pattern, and infill density for each mechanical test, using the geometries and dimensions shown in Figure 1. All specimens were printed flat on their largest face, parallel to the build plate (XY plane), with 4 mm thickness along the build direction (Z axis). Infill line directions were retained at the default settings (45°) of Ultimaker Cura 4.13.1. A total of 270 (5 repetitions × 6 different patterns × 3 different infill densities × 3 different filaments) specimens were manufactured for each test. The specimens were designed according to the UNE-EN ISO 20753:2018 [24] standard, which pertains to the categorization of the dimensions of the different specimens used in the tests. All the tests were performed on a Zwick Z100 universal testing machine (ZwickRoell, Ulm, Germany).

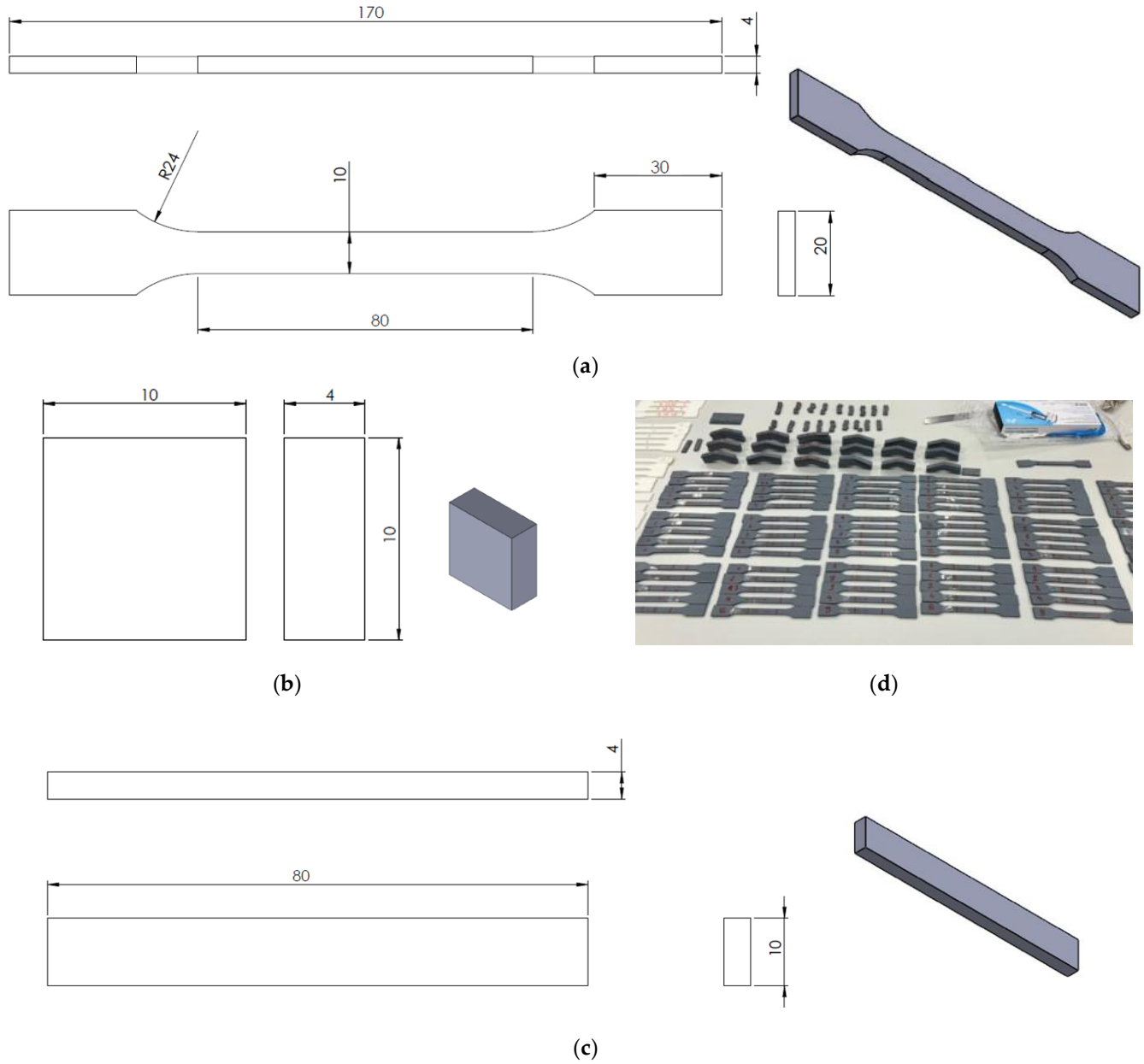


Figure 1. Dimensioned engineering drawings and isometric views of the specimens used for (**a**) tensile, (**b**) compression, and (**c**) flexural testing. All dimensions are in millimetres. (**d**) Some of the printed samples after being tested.

The compressive strength test was performed at a crosshead speed of 10 mm/min until significant non-linear deformation occurred, which was named as CS. In this study, the CS was defined as the stress at the point where this deviation in the stress–strain curve occurred, rather than the maximum stress, due to the polymer's gradual increase in compression resistance without brittle fracture. In relation to the flexural strength test, the crosshead speed was 2 mm/min; the FS was considered as the maximum value of the stress–strain curve. Additionally, the elastic modulus was calculated from the regression line between 30% and 60% of the maximum force, ensuring that the measurements were taken within the elastic region of the material's behaviour. For the tensile strength test, TS was defined as the maximum peak value within the stress–strain curve. The elastic modulus was calculated from the regression line between 20% and 50% of the TS. The crosshead speed was 1 mm/min in the elastic region, and 10 mm/min thereafter. Furthermore, the yield strength was calculated at a 0.2% strain. In the tensile strength test, an extensometer was used to determine the parameters specific to the elastic region. Figure 2 shows

the experimental testing equipment, and Figure 3 presents representative specimens after testing.

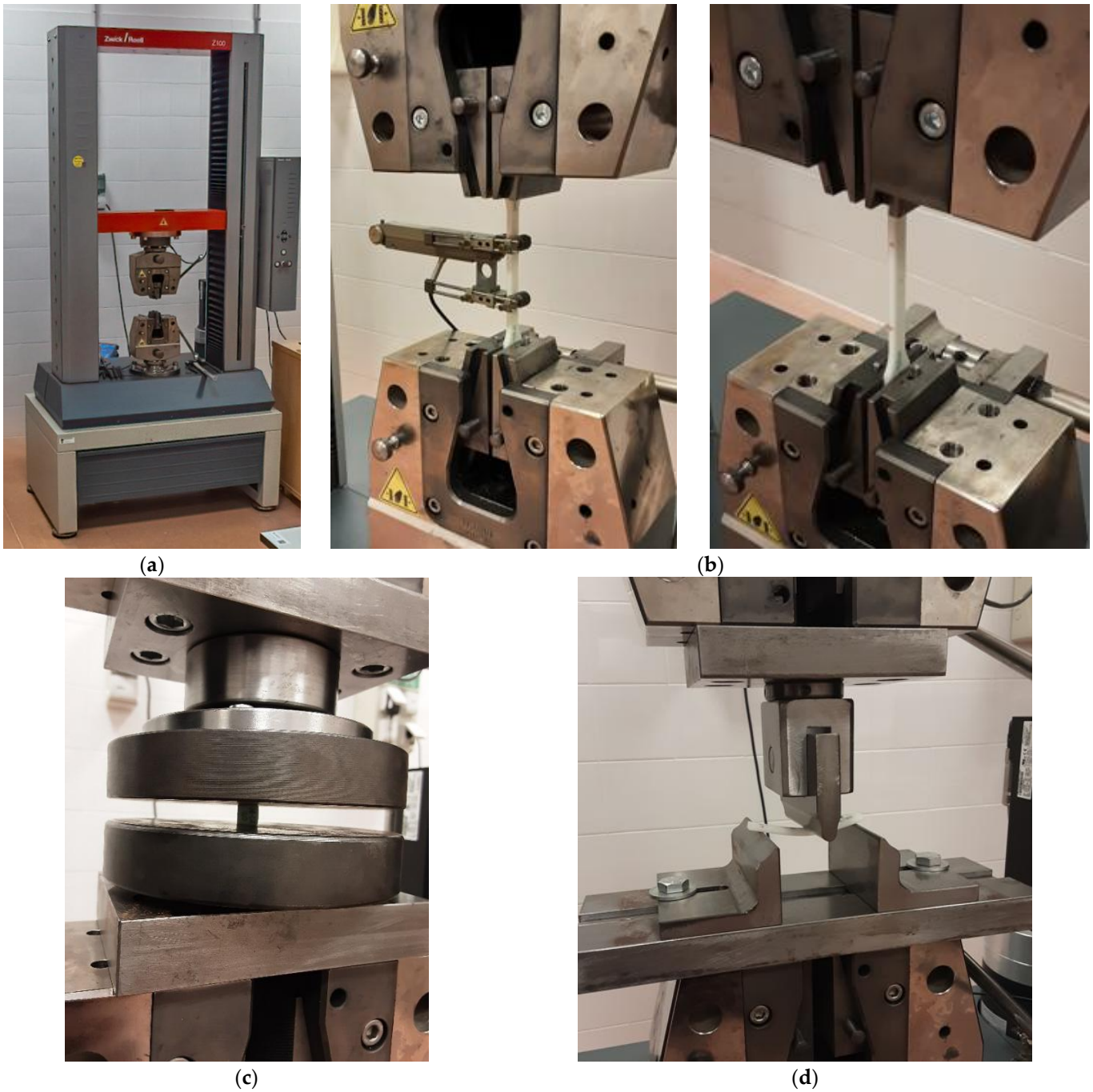


Figure 2. Experimental equipment used for mechanical testing: (**a**) Zwick Z100 universal testing machine; (**b**) tensile testing with details of the extensometer (on the left) and specimen gripping arrangement; (**c**) compression; and (**d**) three-point bending setups.

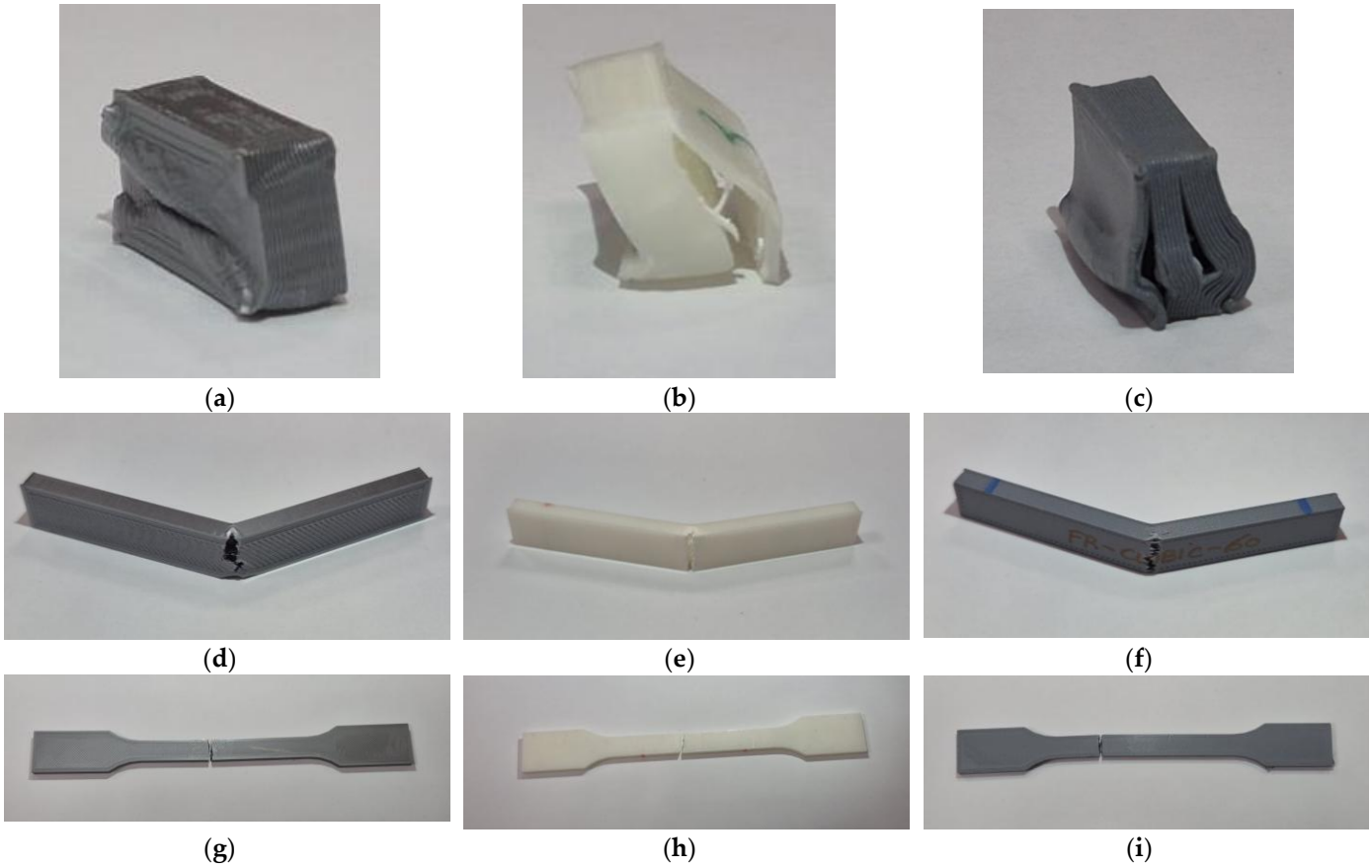


Figure 3. Representative specimens after mechanical testing: (**a**–**c**) compression, (**d**–**f**) three-point bending, and (**g**–**i**) tension. Materials are PLA (**a**,**d**,**g**), ABS (**b**,**e**,**h**), and PETG (**c**,**f**,**i**).

3. Results and Discussion

3.1. Compressive Strength

Figure 4 presents the mean values for the CS. The mean CS values were 51.76 MPa for PLA, 32.12 MPa for ABS, and 32.65 MPa for PETG, indicating that PLA exhibits approximately 60% higher compressive strength compared to ABS and PETG, in agreement with findings from previous studies [13]. Hsueh et al. [25] also reported higher compressive mechanical properties for printed PLA than PETG and demonstrated that printing temperature and speed influence the results. The average coefficient of variation (CV) for CS was 3.6% for PLA, 7.9% for ABS, and 2.6% for PETG. These results suggest that ABS has greater relative variability in CS compared to PLA and PETG. However, its CV value remains within an acceptable range for mechanical testing.

Regarding strain, Ɛ, at CS (Figure 5), the mean values were 0.061 for PLA, 0.063 for ABS, and 0.087 for PETG, with PETG exhibiting approximately 40% higher mean strain at CS than PLA and ABS. This indicates that PETG undergoes greater deformation under compressive loads. The CV for Ɛ at CS was relatively high, at 12.9% for PLA, 19.9% for ABS, and 22.4% for PETG, suggesting greater variability in this measurement.

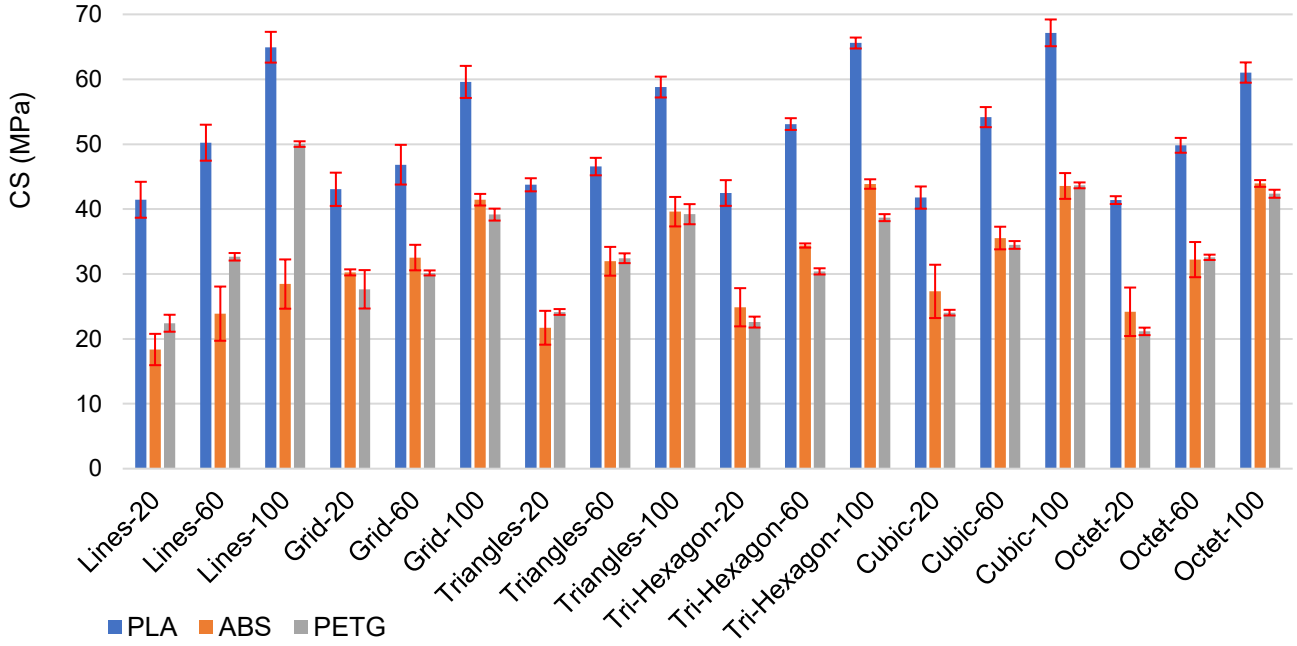


Figure 4. CS.

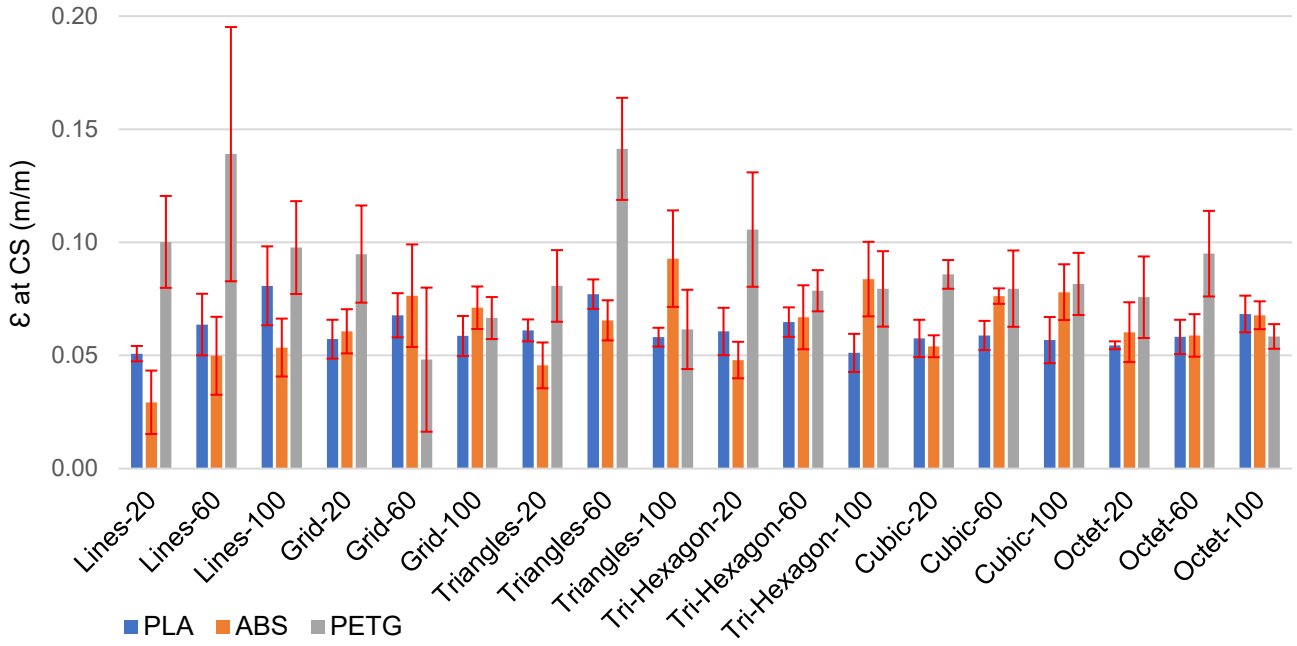


Figure 5. Strain at CS.

3.2. Flexural Strength

The mean FS values shown in Figure 6 were 68.03 MPa for PLA, 45.05 MPa for ABS, and 46.46 MPa for PETG. PLA therefore exhibited more than a 45% increase in strength compared to ABS and PETG, in agreement with previous studies [13]. The higher flexural strength of PLA compared with PETG agrees with the findings of Hsueh et al. [25]. However, since different printing parameters were used for each material, the observed differences may reflect both material characteristics and processing conditions. The coefficient of variation for FS was notably low, at 2.1% for PLA, 1.8% for ABS, and 2.6% for PETG, indicating high consistency in the measurements.

The mean values presented in Figure 7 for the elastic modulus in the flexural strength test were 2435 MPa for PLA, 1596 MPa for ABS, and 1945 MPa for PETG. PLA exhibited approximately 53% higher modulus than ABS and 25% higher modulus than PETG, indicating greater resistance to deformation within the initial flexural response. Although ABS and PETG had similar mean FS values, PETG exhibited an approximately 22% higher flexural modulus. Thus, comparable maximum flexural strengths did not imply equivalent stiffness, an important distinction when selecting materials for components subject to deflection limits. The CV for the elastic modulus was very low, with values of 1.8% for PLA, 2.4% for ABS, and 2.3% for PETG, reflecting high consistency in the measurements across all materials.

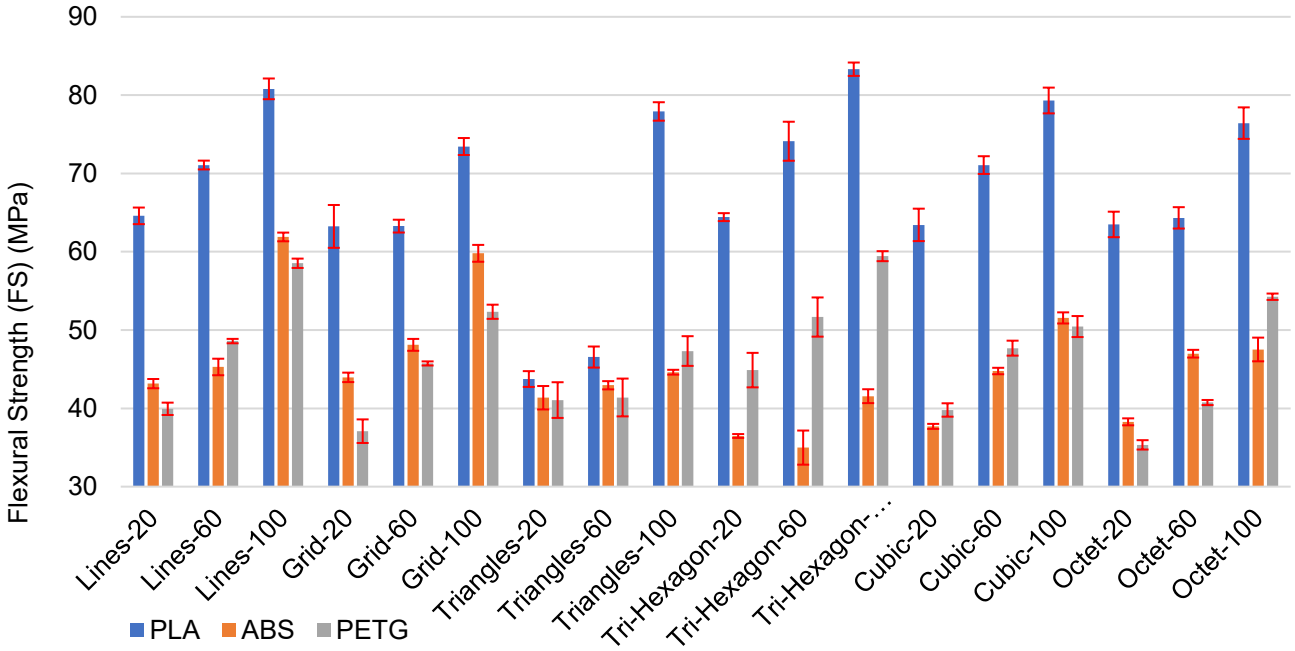


Figure 6. FS.

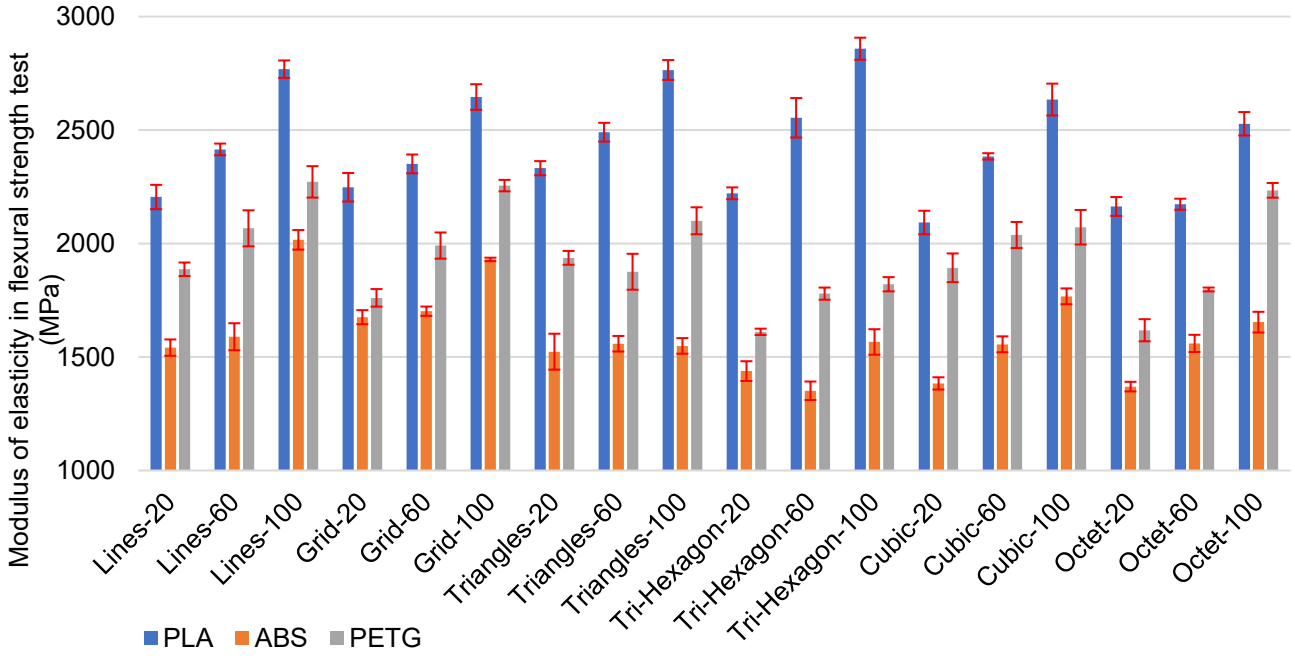


Figure 7. Modulus of elasticity in flexural strength test.

Regarding strain at FS (Figure 8), the mean values were 0.036 for PLA, 0.043 for ABS, and 0.033 for PETG. ABS reached its maximum flexural stress at a greater mean strain than PLA and PETG. Its lower flexural modulus also indicates greater compliance within the initial elastic response. The CV for strain at FS was 2.0% for PLA, 4.5% for ABS, and 4.6% for PETG.

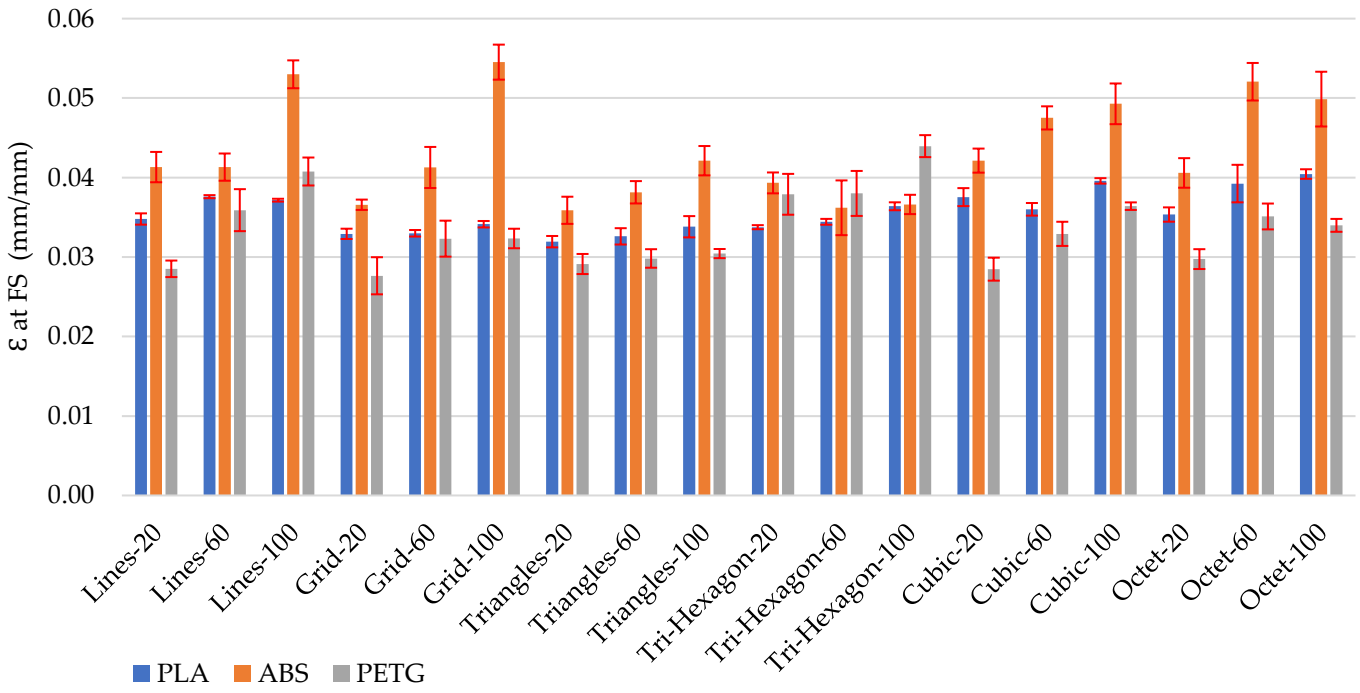


Figure 8. Strain at FS.

3.3. Tensile Strength

The mean values presented in Figure 9 for tensile strength are 36.60 MPa for PLA, 18.56 MPa for ABS, and 21.12 MPa for PETG, indicating approximately 97% higher TS than ABS and 73% higher TS than PETG. PLA exhibited the highest tensile strength, followed by PETG and ABS, consistent with the findings of Erdaş et al. [12] and Menargues et al. [17] under their respective experimental conditions. The coefficient of variation for tensile strength was 4.2% for PLA, 1.8% for ABS, and 4.5% for PETG, indicating low relative scatter within the filament material groups.

The mean strains at TS (Figure 10) were similar for all three materials, with mean values of 0.013 for PLA, 0.011 for ABS, and 0.011 for PETG. The coefficient of variation for this property was low, being 4.6% for PLA, 2.2% for ABS, and 10.9% for PETG. The elastic modulus in tensile strength (Figure 11) was 4016 MPa for PLA, 2898 MPa for ABS, and 3153 MPa for PETG, showing a pattern similar to that observed in flexural strength, with low coefficients of variation (2.7% ± 0.2). D'Andrea et al. [26] reported that PLA exhibits a higher elastic modulus than ABS independently of the printing orientation. Additionally, yield strength was studied (Figure 12), with the mean values being 29.14 MPa for PLA, 16.65 MPa for ABS, and 17.64 MPa for PETG, indicating a greater than 65% increase in PLA's yield strength compared to both ABS and PETG. The higher yield strength of PLA was accompanied by a broadly comparable strain at yield, consistent with its greater initial stiffness. The coefficient of variation for yield strength was very low, at 3.6% for PLA, 1.8% for ABS, and 2.7% for PETG. The strain at yield strength (Figure 13) was similar for all materials, with a mean value of 0.0075 ± 0.0005, and a low CV of 2.7% ± 0.4.

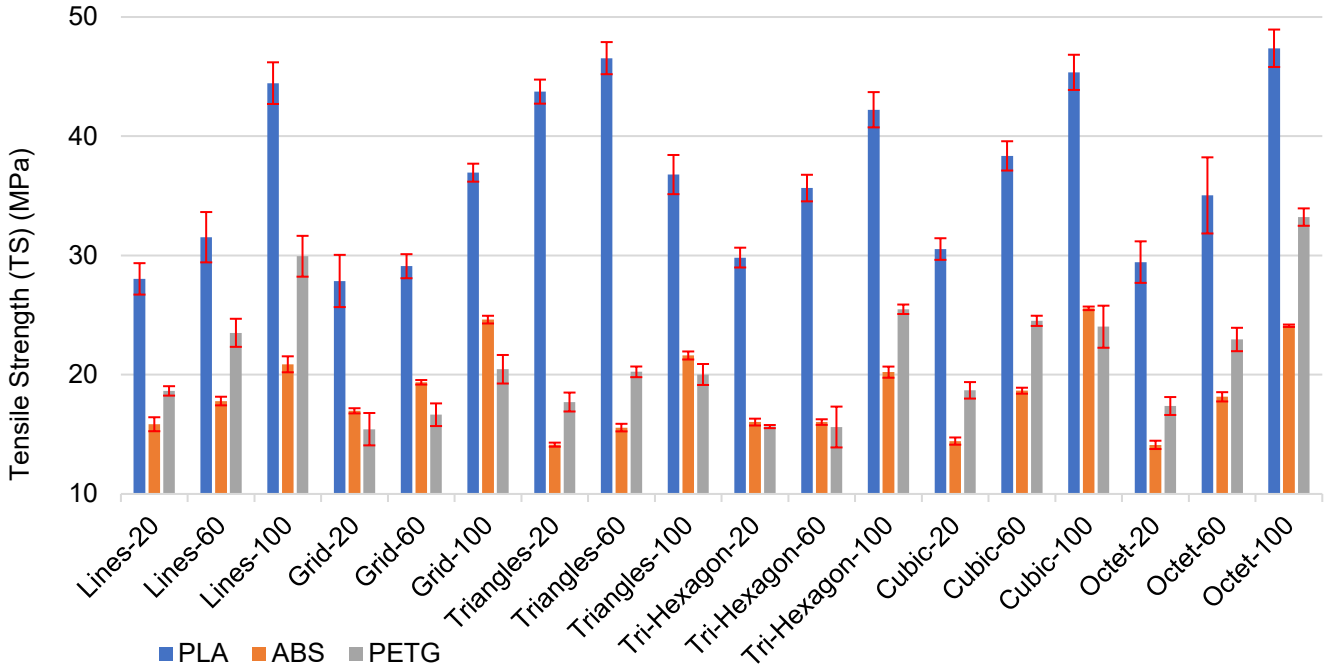


Figure 9. TS.

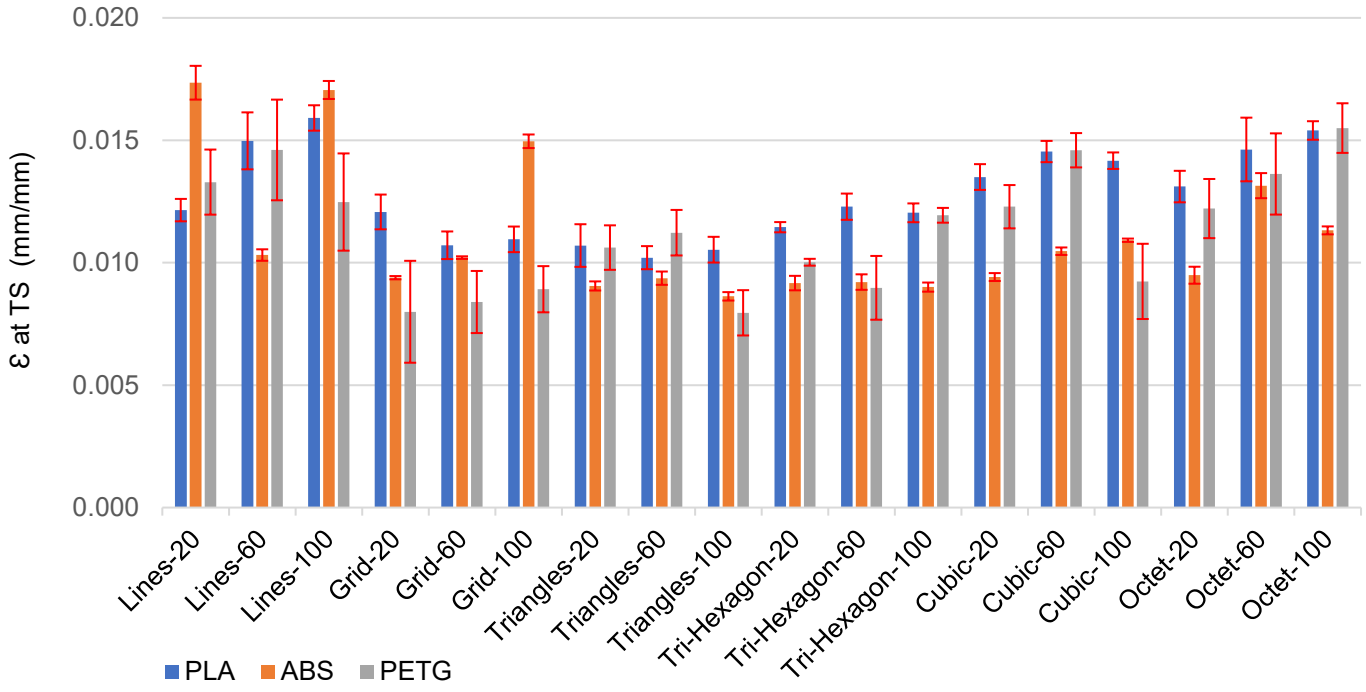


Figure 10. Strain at TS.

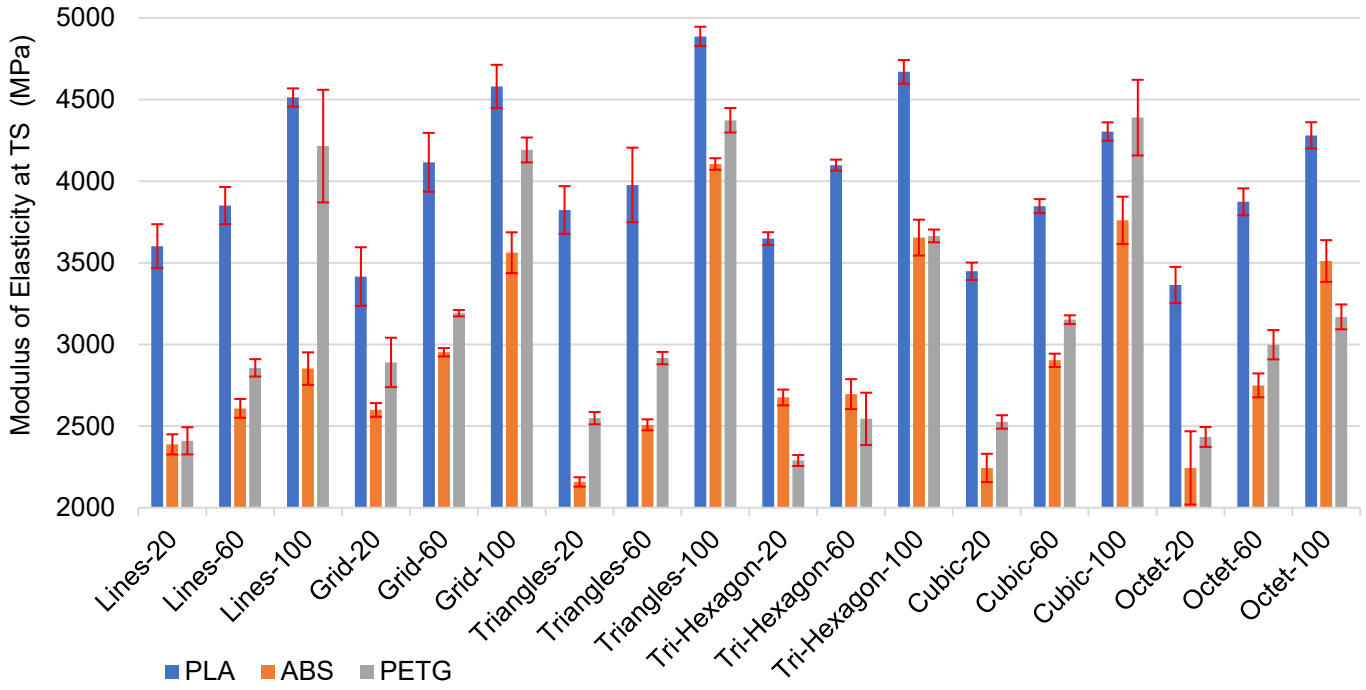


Figure 11. Modulus of elasticity in tensile strength test.

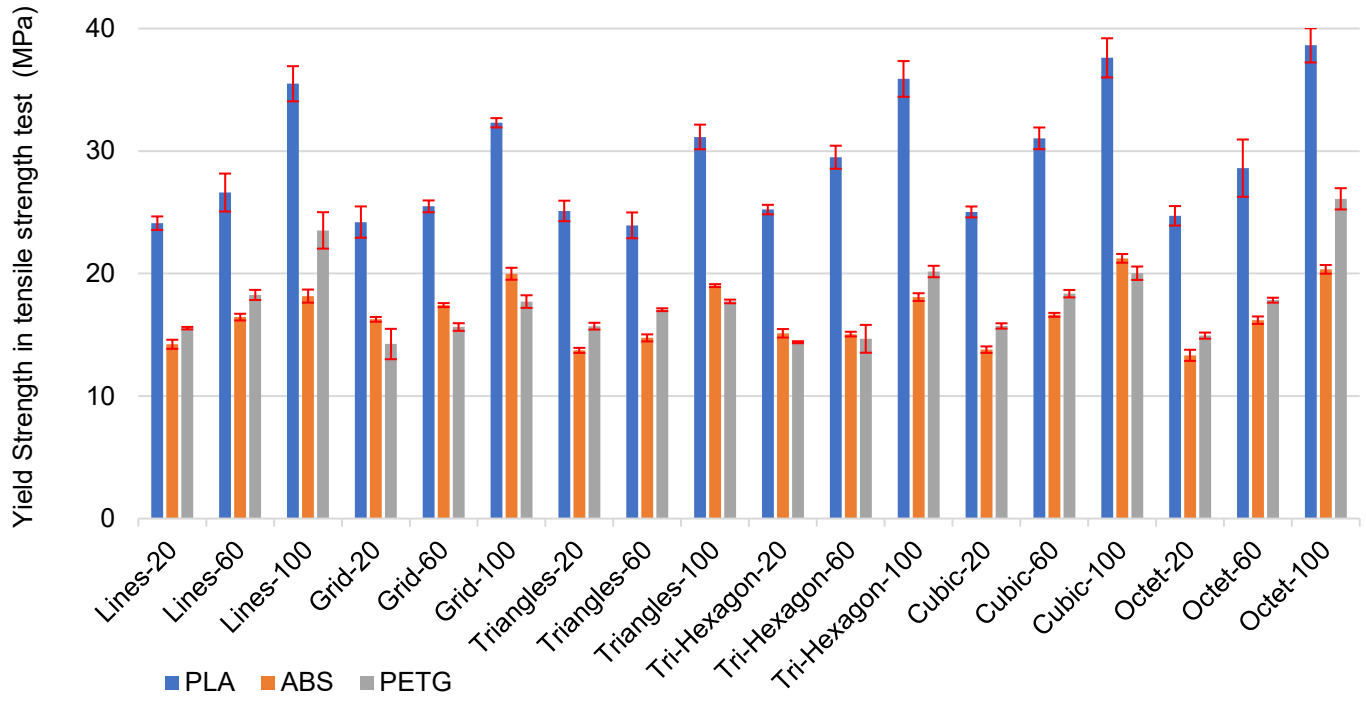


Figure 12. Yield strength in tensile strength test.

https://doi.org/10.3390/jmmp10120533

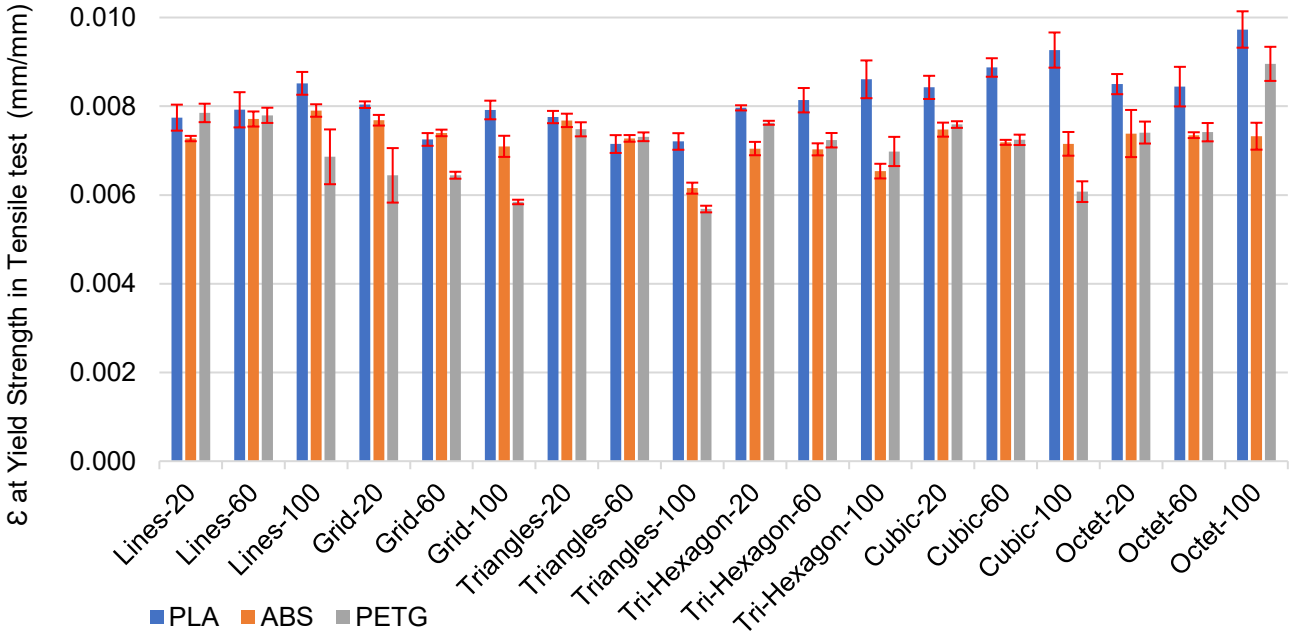


Figure 13. Strain at yield strength in tensile strength test.

4. Statistical Analysis

Since the aim of this study is to optimize the mechanical properties of the different materials studied for 3D printing, the statistical analysis focused on compressive (CS), flexural (FS), and tensile strength (TS) to assess the influence of infill density and pattern. Although the experimental design included multiple factors, the statistical comparisons focused on identifying the best-performing infill patterns within each fixed material–density combination and loading mode. Separate one-way ANOVAs, with infill pattern as the factor, were therefore followed, where appropriate, by Hsu's Multiple Comparisons with the Best. This approach provides condition-specific comparisons but does not quantify interactions among material, infill density, and pattern. Consequently, the results are interpreted within each investigated condition rather than as estimates of independent factor effects.

Initially, a one-way ANOVA was performed for each material and loading mode to assess differences in strength among infill-density levels. In each of these analyses, the degrees of freedom were reported as two for the infill density factor, 87 for the error, and 89 for the total. This corresponds to 90 measurements for each filament (PLA, ABS, and PETG), with 30 measurements at each infill density. In analyses where outliers were excluded, the number of replicates per group was reduced to a minimum of three. The statistical calculations were performed using Minitab 19 software. The results confirmed, as expected, that infill density significantly affected strength in all analyses ($p < 0.001$). This was also found by Algarny and Ghazali [27], who studied the mechanical properties of PLA, ABS and PETG filaments, among others. After establishing the significant influence of infill density, the analysis proceeded to evaluate the effect of infill pattern at each density level. Subsequently, one-way ANOVA was conducted to evaluate the effect of the pattern as a single factor, for each of the infill densities and filaments.

After this, to further investigate the effect of the pattern, a statistical analysis using Hsu's MCB method was performed. The MCB approach allowed for the identification of the best-performing infill pattern for each infill density and each material and mechanical test. It is a powerful test when comparison is performed between the group with the highest or lowest means and the other groups [28]. The one-way ANOVA conducted to

evaluate the effect of the infill pattern as a single factor for each infill density revealed a *p*-value < 0.001 for all of them except for PLA at 20% infill, where no significant differences were detected for CS (*p*-value = 0.604), FS (*p*-value = 0.949), or TS (*p*-value = 0.056). In each of these 27 ANOVAs, the degrees of freedom were reported as 5 for the pattern factor, 24 for the error, and 29 for the total (except in some cases where outliers were removed as mentioned before). For the ANOVA plots, the confidence intervals (CI) were calculated using the pooled standard deviation from the analysis, ensuring consistent variance estimation across groups.

MCB plots show 95% simultaneous confidence intervals for differences relative to the best-performing group. Intervals crossing zero indicate no statistically significant difference. When the *p*-value was greater than 0.05, for PLA at 20% infill in CS, FS and TS, MCB post hoc analysis was not applied and only descriptive statistics of group performance are provided.

The statistical analysis set the basis for providing practical recommendations for optimizing 3D printing parameters based on targeted mechanical requirements, as later will be seen in Section 5.

4.1. Compressive Strength

Compressive strength increased markedly with infill density for all filaments (Figures 14a, 15a and 16a). PLA exhibited the highest CS (≈52 MPa), about 60% higher than ABS and PETG (~32 MPa each), consistent with its greater stiffness. The effect of infill density was most pronounced for PETG and ABS, which showed gains of 65–80% from 20% to 100% infill.

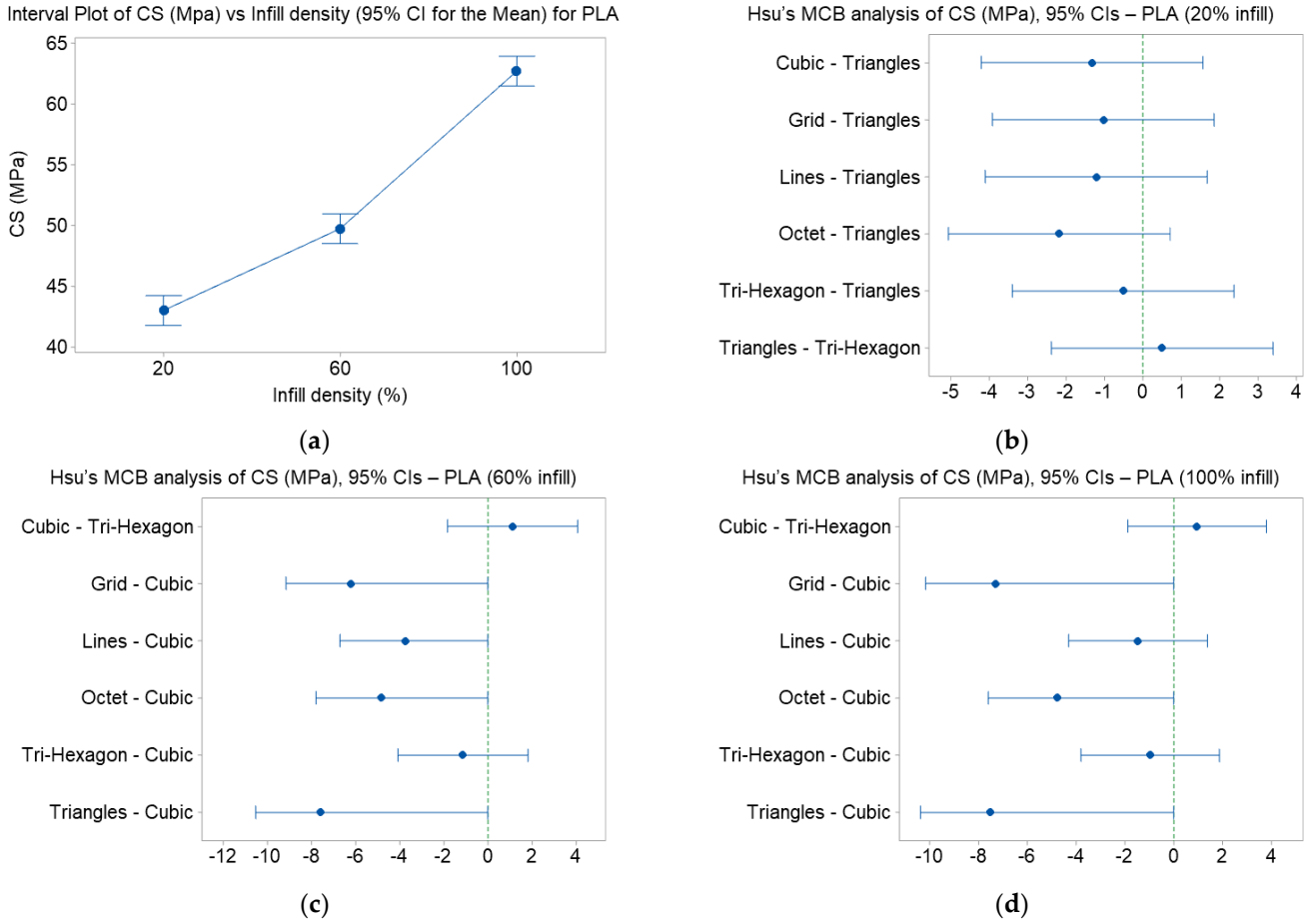


Figure 14. Statistical analysis for CS and for PLA filaments: (**a**) one-way ANOVA for CS and infill density; Hsu's MCB analysis for an infill density of (**b**) 20% (**c**) 60% and (**d**) 100%.

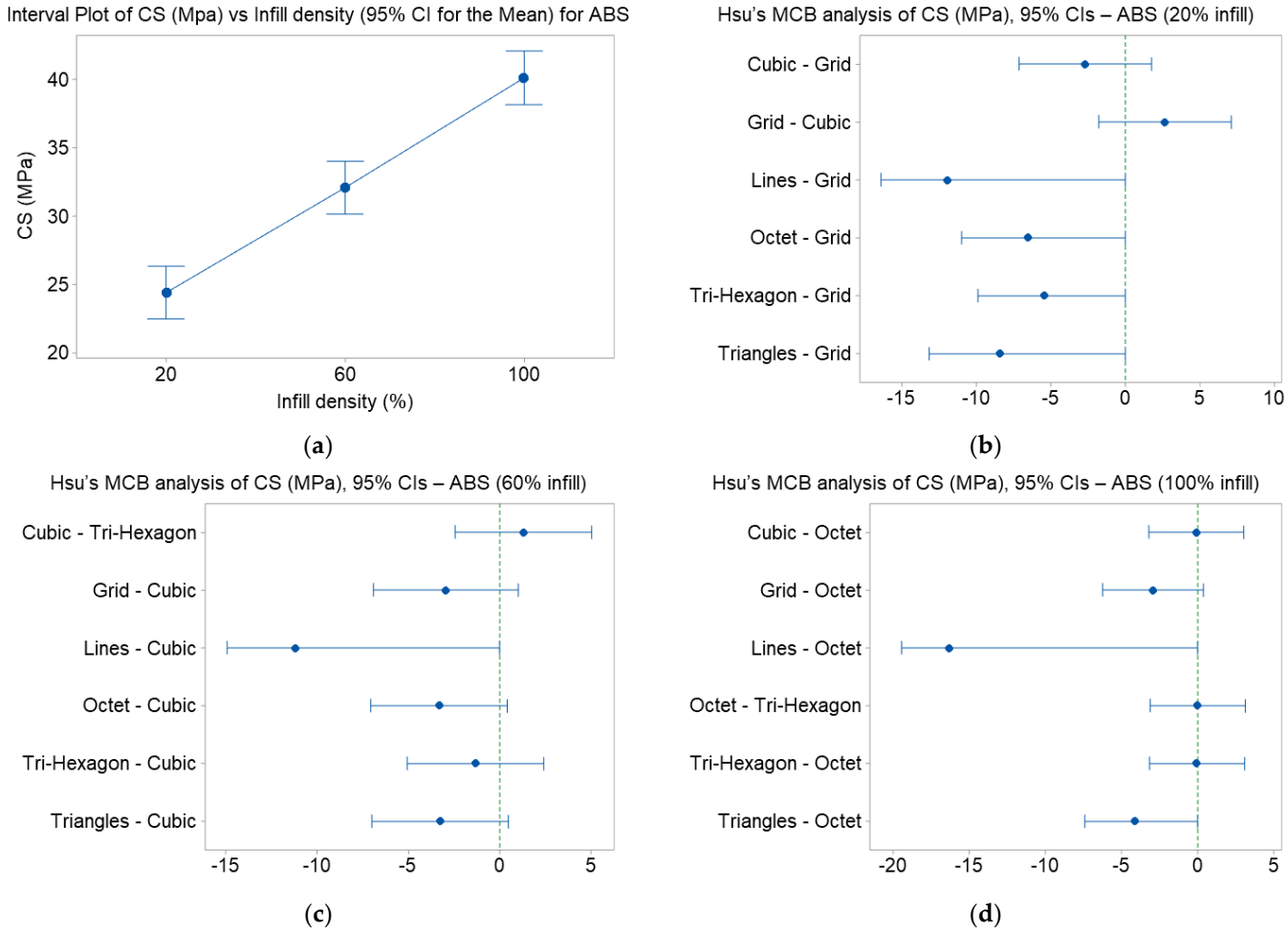


Figure 15. Statistical analysis for CS and for ABS filaments: (**a**) one-way ANOVA for CS and infill density; Hsu's MCB analysis for an infill density of (**b**) 20%, (**c**) 60%, and (**d**) 100%.

Hsu's MCB analysis revealed that the optimal infill pattern depended on both density and material (Figures 14b–d, 15b–d and 16b–d). For PLA, the Tri-Hexagon pattern consistently achieved the best or statistically equivalent results across all densities. For ABS, the optimal pattern changed with density—Grid (20%), Cubic (60%), and Octet (100%)—while for PETG, Grid (20%), Cubic (60%), and Lines (100%) were preferred. Overall, Cubic and Grid geometries provided robust compressive performance, whereas the simple Lines pattern yielded the lowest strength values.

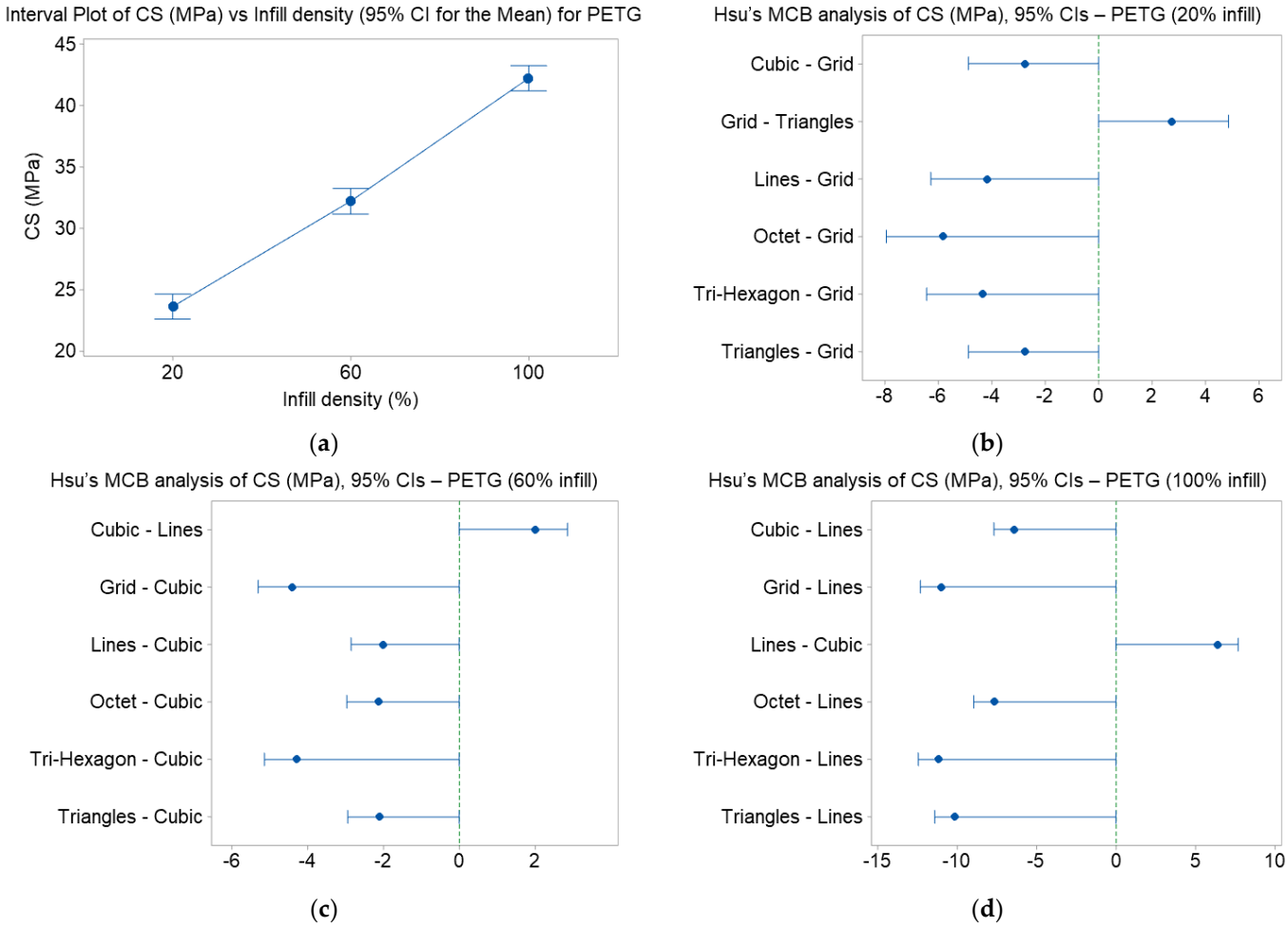


Figure 16. Statistical analysis for CS and for PETG filaments: (**a**) one-way ANOVA for CS and infill density; Hsu's MCB analysis for an infill density of (**b**) 20%, (**c**) 60%, and (**d**) 100%.

4.2. Flexural Strength

Flexural strength increased moderately with infill density—typically 20–35% from 20% to 100% (Figures 17a, 18a and 19a). PLA again showed the highest FS (≈79 MPa), followed by PETG (≈54 MPa) and ABS (≈51 MPa).

The influence of infill pattern depended on the material and density (Figures 17b–d, 18b–d and 19b–d). The Tri-Hexagon pattern achieved the highest or statistically equivalent FS for PLA and PETG at all investigated densities. For ABS, Grid performed best at 20–60% infill, while Lines exhibited a slightly higher mean FS at 100% infill. These differences may be associated with the influence of infill geometry on stress distribution and load transfer under bending. The Lines pattern was favourable at high density for ABS, which exhibited the lowest flexural modulus under the investigated conditions, suggesting that its performance reflects the combined influence of material response and infill geometry.

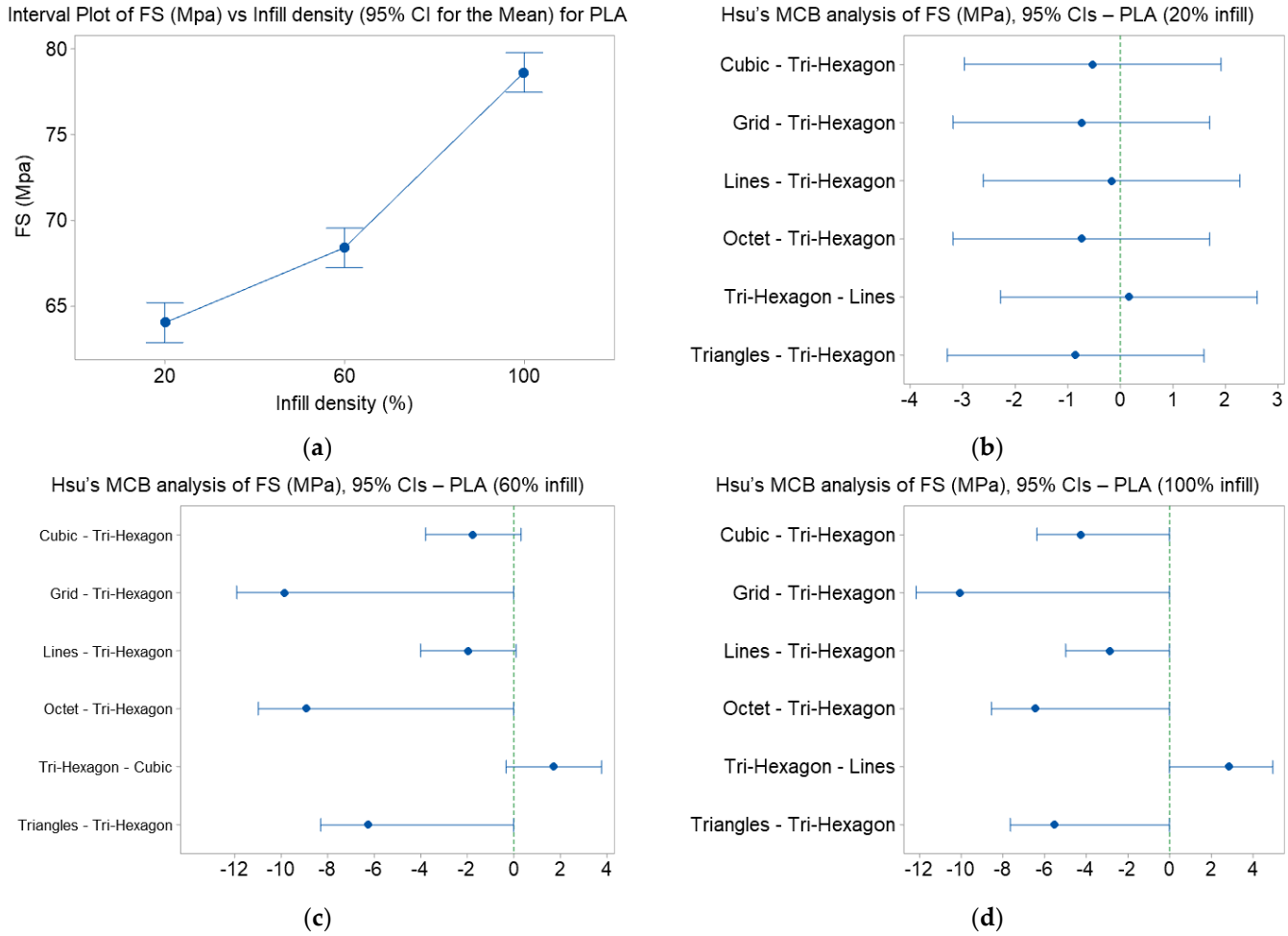
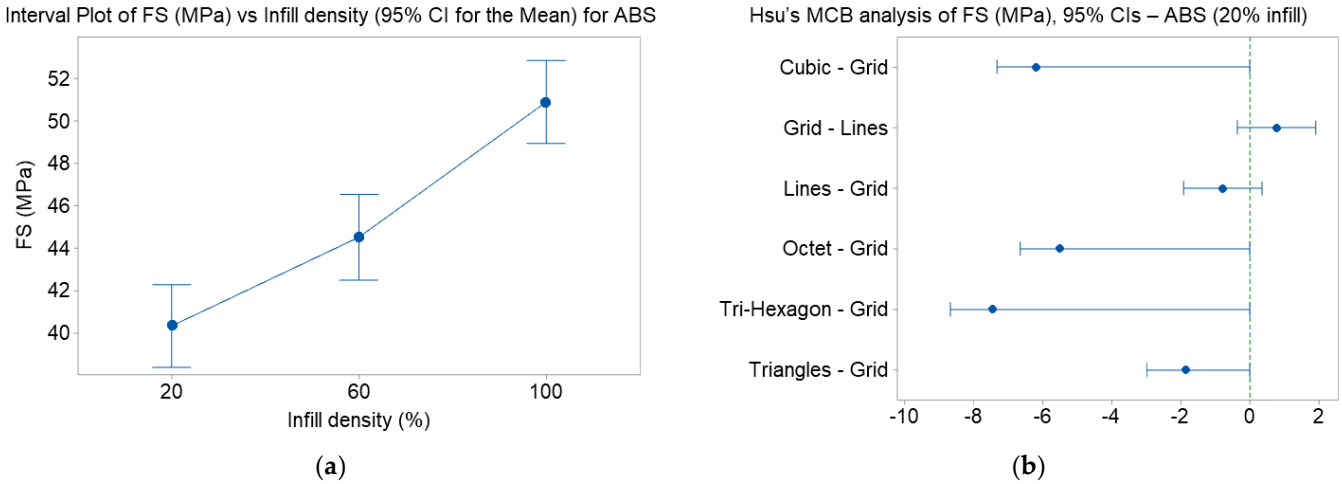


Figure 17. Statistical analysis for FS and for PLA filaments: (**a**) one-way ANOVA for FS and infill density; Hsu's MCB analysis for an infill density of (**b**) 20% (**c**) 60% and (**d**) 100%.



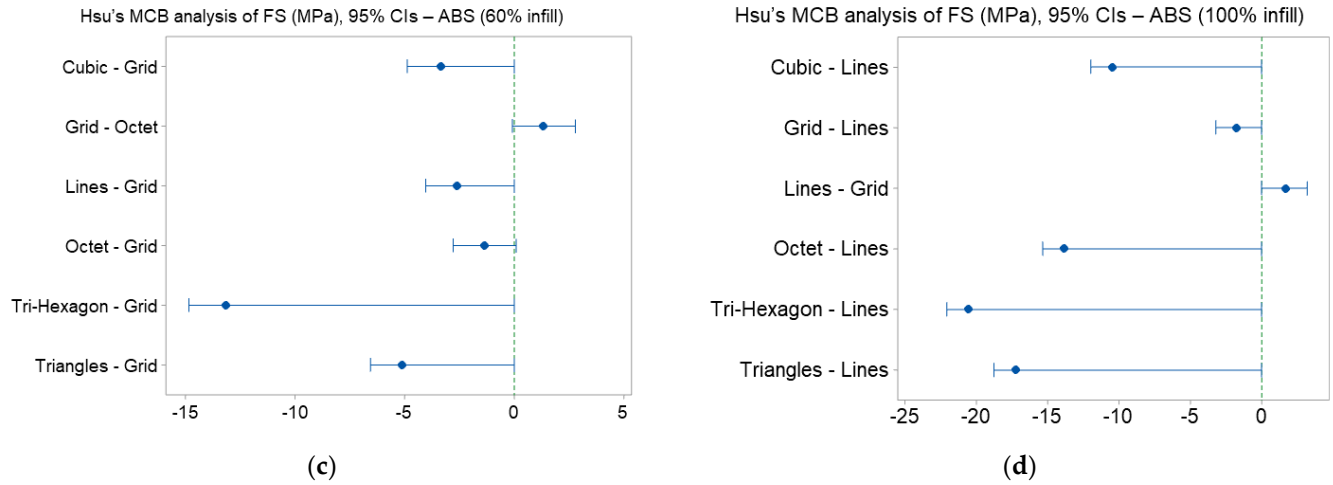


Figure 18. Statistical analysis for FS and for ABS filaments: (**a**) one-way ANOVA for FS and infill density; Hsu's MCB analysis for an infill density of (**b**) 20% (**c**) 60% and (**d**) 100%.

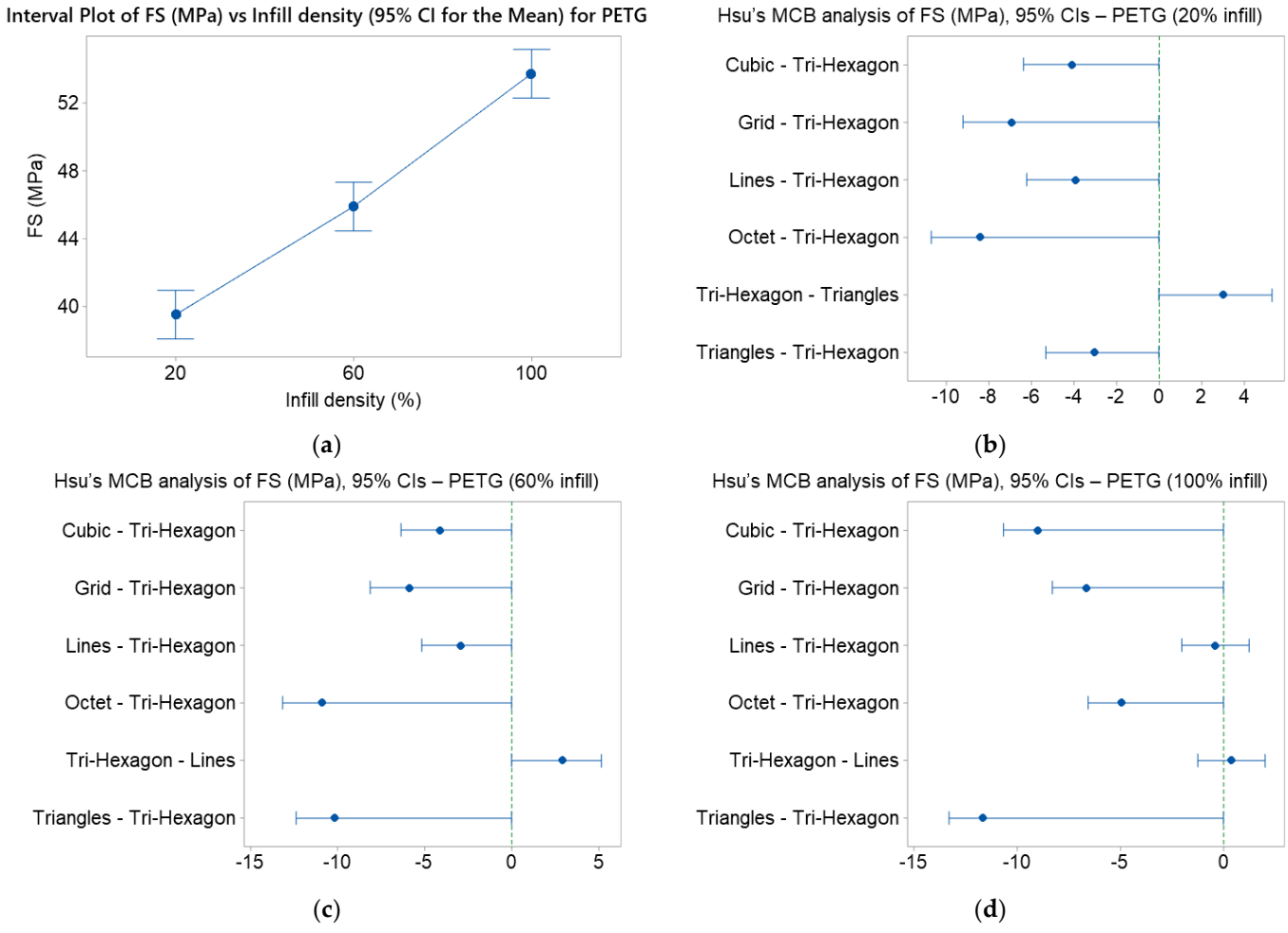


Figure 19. Statistical analysis for FS and for PETG filaments: (**a**) one-way ANOVA for FS and infill density; Hsu's MCB analysis for an infill density of (**b**) 20%, (**c**) 60%, and (**d**) 100%.

4.3. Tensile Strength

Tensile strength exhibited an almost linear dependence on infill density (Figures 20a, 21a and 22a). Strength rose by 40–60% from 20% to 100% infill. PLA reached the highest TS (≈42 MPa), nearly double that of ABS (≈22 MPa) and significantly higher than PETG (≈27 MPa).

According to Hsu's MCB results, the Cubic and Octet patterns provided the best tensile performance (Figures 20b–d, 21b–d and 22b–d). For PLA, Cubic dominated up to 60% infill, after which Octet became superior. ABS showed a transition from Lines (≤60%) to Cubic (≥60%), while PETG followed a similar evolution (Lines → Cubic → Octet) as density increased; Daly et al. [29] also found a significant increase between 20% and 100% of infill density. These changes highlight that open lattice geometries such as Cubic and Octet distribute axial stresses more effectively, while denser grid-based patterns favour compressive and flexural loading.

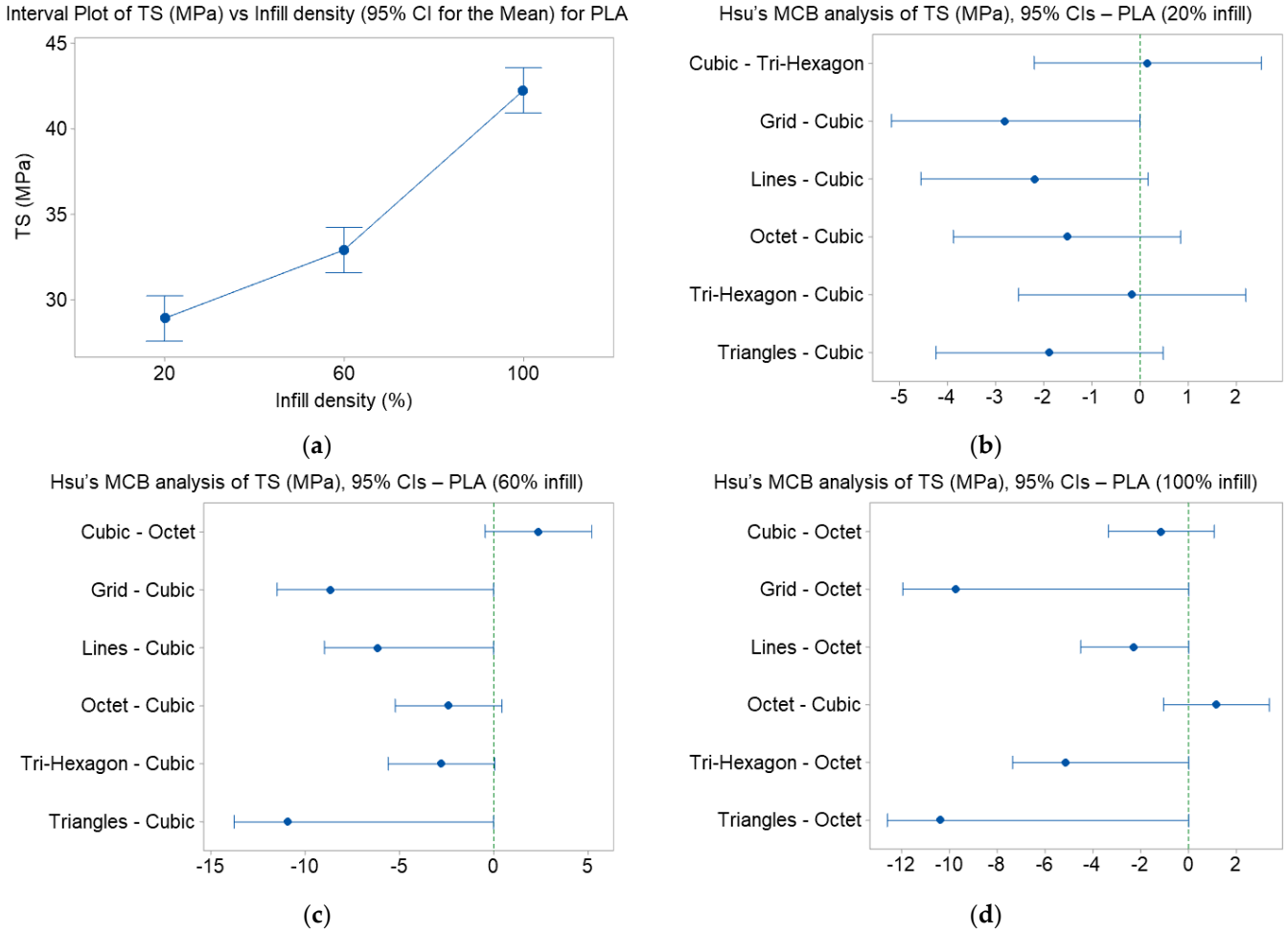
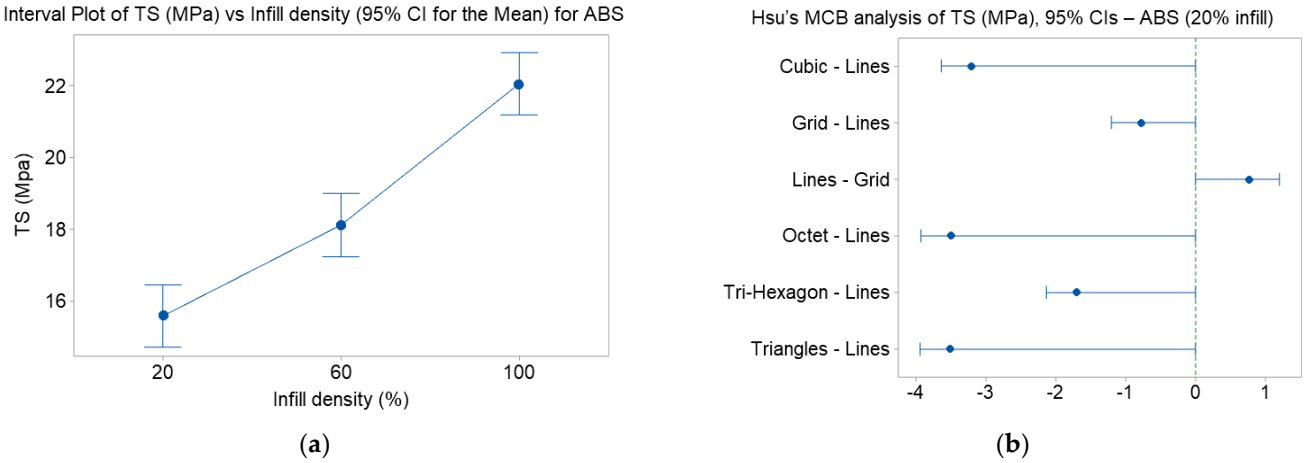


Figure 20. Statistical analysis for TS and for PLA filaments: (**a**) one-way ANOVA for TS and infill density; Hsu's MCB analysis for an infill density of (**b**) 20%, (**c**) 60% and (**d**) 100%.



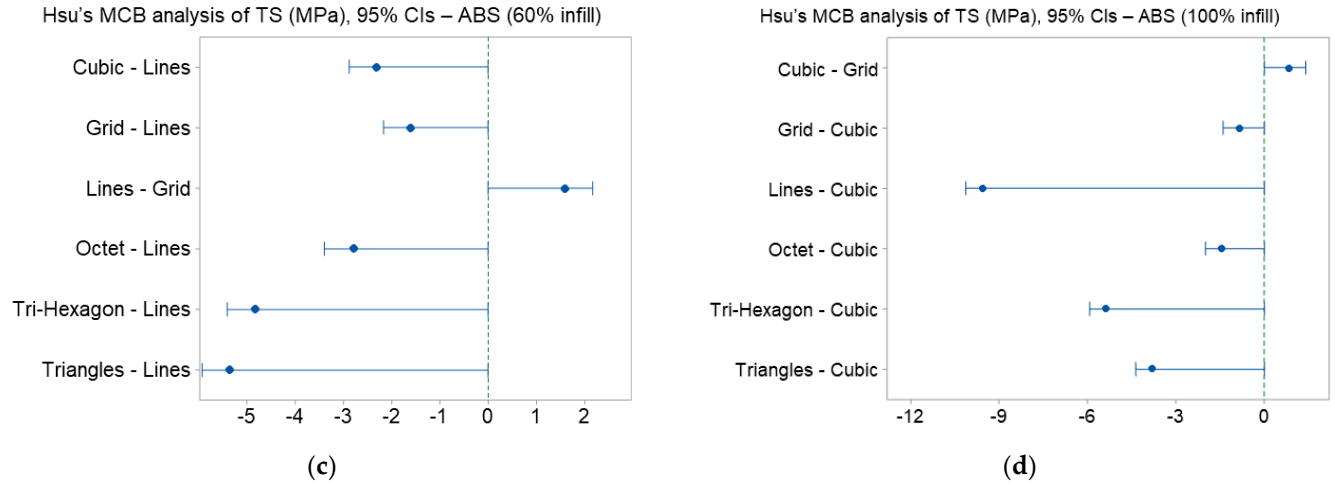


Figure 21. Statistical analysis for TS and for ABS filaments: (**a**) one-way ANOVA for TS and infill density; Hsu's MCB analysis for an infill density of (**b**) 20% (**c**) 60% and (**d**) 100%.

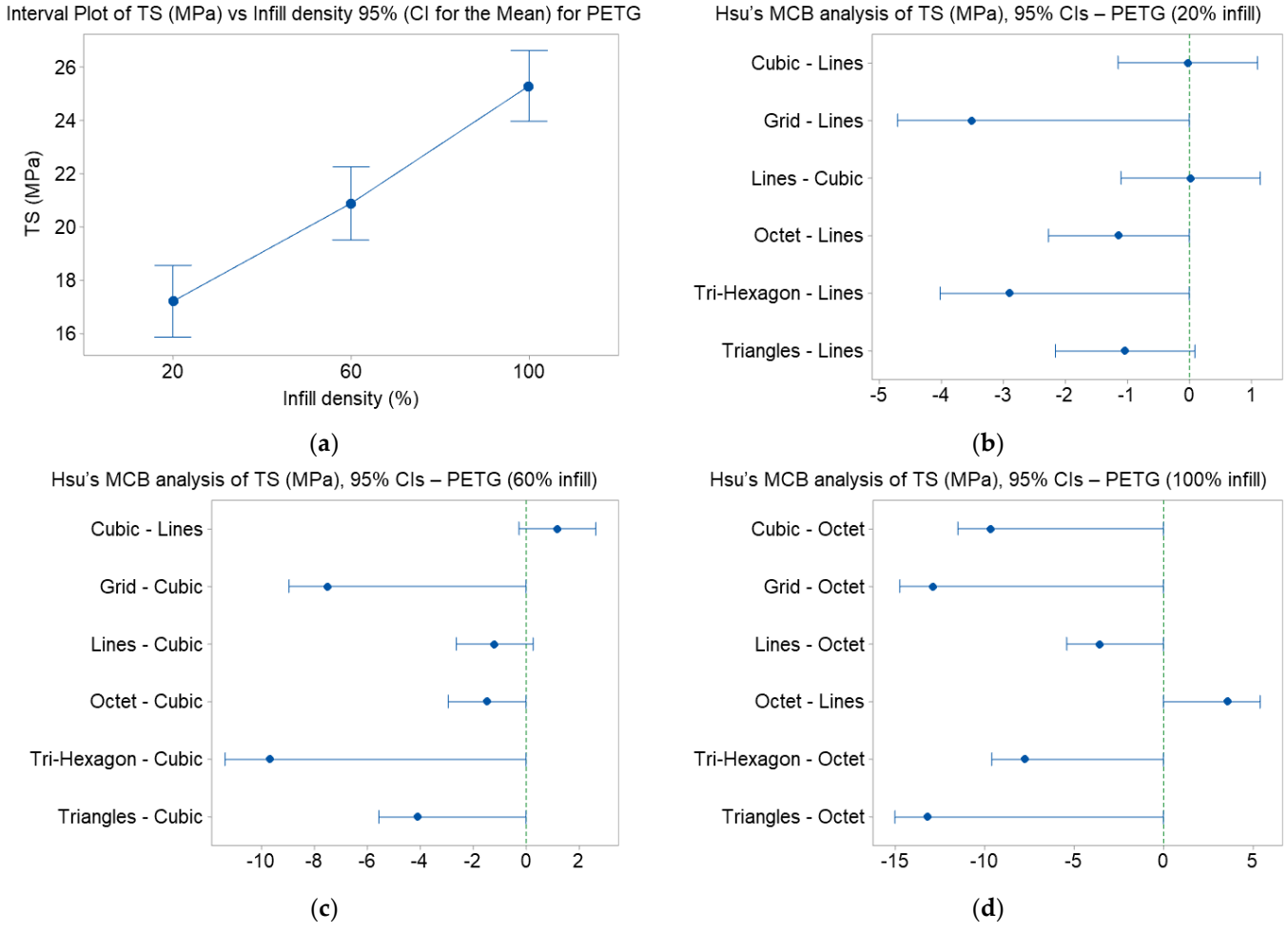


Figure 22. Statistical analysis for TS and for PETG filaments: (**a**) one-way ANOVA for TS and Infill density; Hsu's MCB analysis for an infill density of (**b**) 20% (**c**) 60% and (**d**) 100%.

5. Optimizing the Mechanical Properties

Linear regression models relating strength to infill density were developed from 15 data points (five replicates at each of the three infill-density levels). The regression coefficients are summarized in Table 2. Of the 54 models, 44 yielded $R^2 \geq 0.859$, and only 2 had $R^2 < 0.740$. These values characterize the fit to the experimental data. Intermediate density

estimates and calculated pattern crossover points are conditional on the assumed linear relationships and provide preliminary guidance within the investigated density range and processing conditions.

The highest strengths were obtained at 100% infill; therefore, this density is appropriate when maximizing strength is the sole objective. The practical purpose of the proposed framework is to support infill selection for a specified strength requirement. Infill density governs the overall strength trend, while pattern selection provides an additional means of adjusting performance at a given density, depending on the material and loading mode. A favourable pattern may therefore meet a target strength at a lower nominal density than a less favourable pattern. This offers potential benefits in material consumption and printing efficiency, although reductions in nominal infill density do not translate directly into equivalent reductions in total specimen mass or printing time because walls, outer layers, and toolpath characteristics also contribute. This framework provides preliminary strength-based selection guidance.

Table 2. Slope, intercept and coefficient of determination for the linear regressions for each pattern and material.

		CS			FS			TS		
Material	**Pattern**	**m ***	**n ****	**R^2 *****	**m ***	**n ****	**R^2 *****	**m ***	**n ****	**R^2 *****
PLA	Lines	0.282	35.639	0.956	0.203	59.922	0.987	0.207	22.511	0.931
	Grid	0.206	37.467	0.925	0.120	59.659	0.799	0.122	24.109	0.900
	Triangles	0.153	40.472	0.745	0.178	58.864	0.945	0.102	24.622	0.741
	Tri-Hexagon	0.279	37.068	0.990	0.236	59.551	0.983	0.146	27.024	0.974
	Cubic	0.301	36.167	0.987	0.190	60.185	0.972	0.194	26.455	0.985
	Octet	0.253	35.610	0.985	0.165	58.466	0.855	0.227	23.540	0.955
ABS	Lines	0.119	16.375	0.765	0.228	36.280	0.907	0.062	14.481	0.958
	Grid	0.134	26.703	0.936	0.204	38.475	0.959	0.097	14.495	0.974
	Triangles	0.228	17.812	0.955	0.033	41.249	0.785	0.094	11.505	0.936
	Tri-Hexagon	0.241	19.929	0.981	0.064	34.006	0.749	0.052	14.293	0.865
	Cubic	0.206	23.385	0.936	0.172	34.293	0.997	0.138	11.262	0.988
	Octet	0.255	18.070	0.958	0.121	37.114	0.901	0.124	11.440	0.992
PETG	Lines	0.340	14.744	0.985	0.235	35.045	0.997	0.137	15.577	0.968
	Grid	0.150	23.195	0.926	0.194	33.428	0.987	0.065	13.498	0.887
	Triangles	0.195	20.467	0.989	0.082	38.309	0.751	0.030	17.486	0.698
	Tri-Hexagon	0.202	18.466	0.996	0.190	40.125	0.962	0.121	11.937	0.859
	Cubic	0.242	19.612	0.997	0.129	38.079	0.942	0.061	18.485	0.723
	Octet	0.265	16.102	0.997	0.234	29.412	0.966	0.196	12.740	0.980

* Slope, ** intercept and *** coefficient of determination of the linear regressions.

5.1. Compressive Strength

Figure 23 shows the best-performing pattern regression lines for CS as a function of infill density. The intersections indicate the estimated densities at which the predicted best-performing pattern changes. For PLA filaments, Figure 23a shows that below 18.4% infill density, the Triangles pattern exhibits the highest compressive strength, whereas above this threshold, the Cubic pattern provides superior performance. For ABS (Figure 23b), Grid provided the highest predicted CS up to an infill density of approximately 46.4%, while Cubic performed best above this density within the investigated range. The Cubic and Octet regression lines intersect at approximately 108% infill, outside the physically feasible range; therefore, Octet was not selected by the regression-based procedure. Figure 23c shows that up to an infill density of 38.7%, the Grid pattern exhibited the best performance. Between 38.7% and 49.8%, the Cubic pattern was superior, while beyond

this point, the Lines pattern showed the best performance for PETG filaments. Figure 23d shows an example for predicting the required infill density to achieve a target compressive strength (e.g., 45.9% infill for 50 MPa).

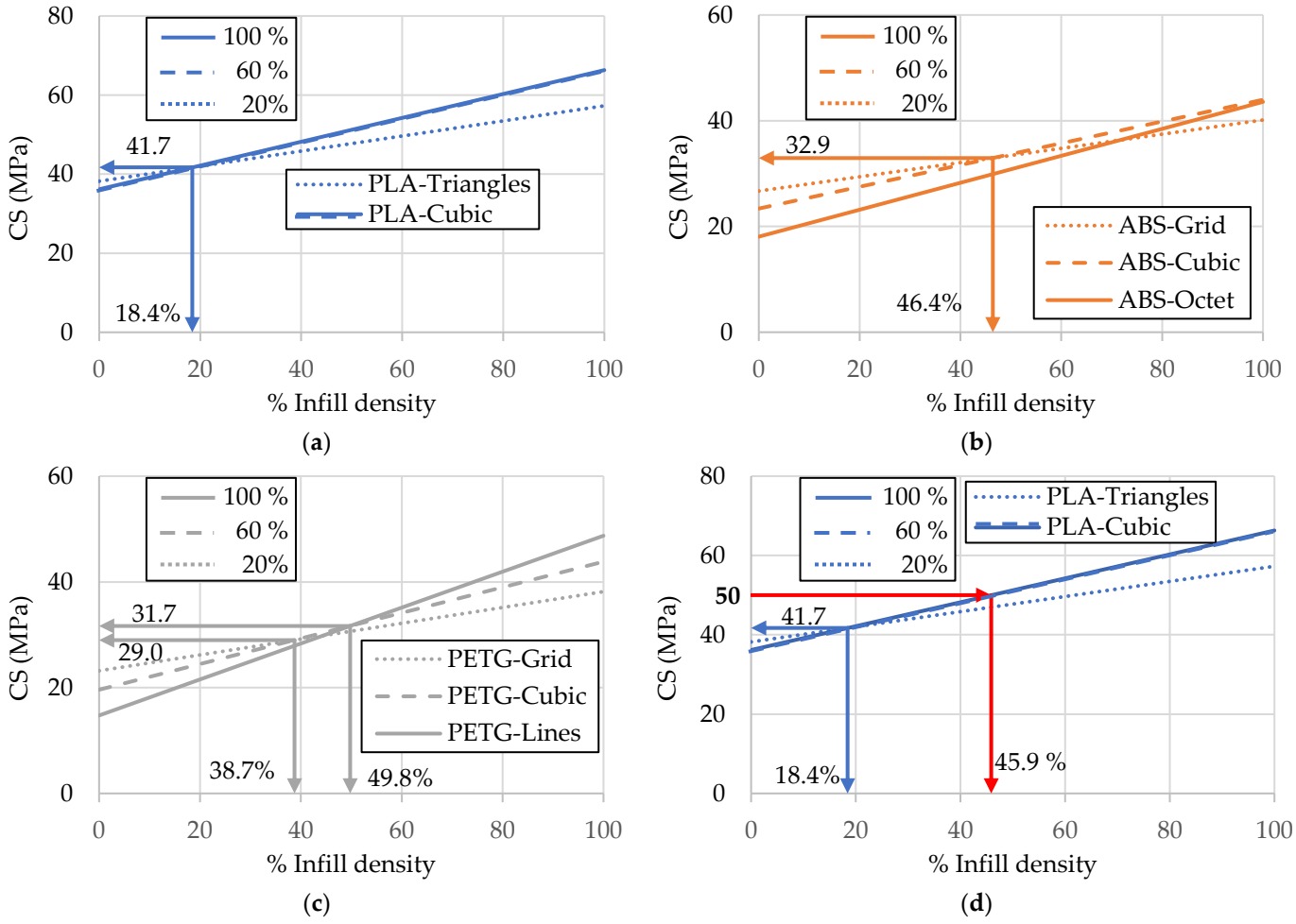


Figure 23. Regression lines for the predicted best-performing patterns for CS as a function of infill density for (**a**) PLA, (**b**) ABS, (**c**) PETG and (**d**) an example for the determination of the best pattern and infill density for a CS target, in this case 50MPa, for the PLA filament.

5.2. Flexural Strength

Figure 24 shows the regression lines for the predicted best-performing patterns for FS as a function of infill density. It also shows that the intersection points indicate the threshold density at which one pattern outperforms another. For PLA filaments, Figure 24a shows that the Tri-Hexagon exhibited the best performance for the three infill densities studied. In the case of ABS (Figure 24b), up to an infill density of 90.6%, Grid was the best pattern; above this density, Lines had the highest predicted FS. For PETG, the Tri-Hexagon pattern provided the highest predicted flexural strength throughout the investigated infill-density range (Figure 24c). Figure 24d shows an example for predicting the required infill density to achieve a target flexural strength (e.g., 44.2% infill for 70 MPa) for the PLA filament, which is the most used. As an illustration, consider a shelf-like PLA support with the same dimensions as the flexural specimen (L = 64 mm, b = 10 mm, d = 4 mm). For a service load of F = 58 N and a safety factor n = 2, the maximum stress from three-point bending is 70 MPa (Equation (1)). Using the regression chart, this stress requirement corresponds to an infill density of 44.2% (Figure 24d):

$$FS = \frac{3FL}{2bd^2} \times n, \quad (1)$$

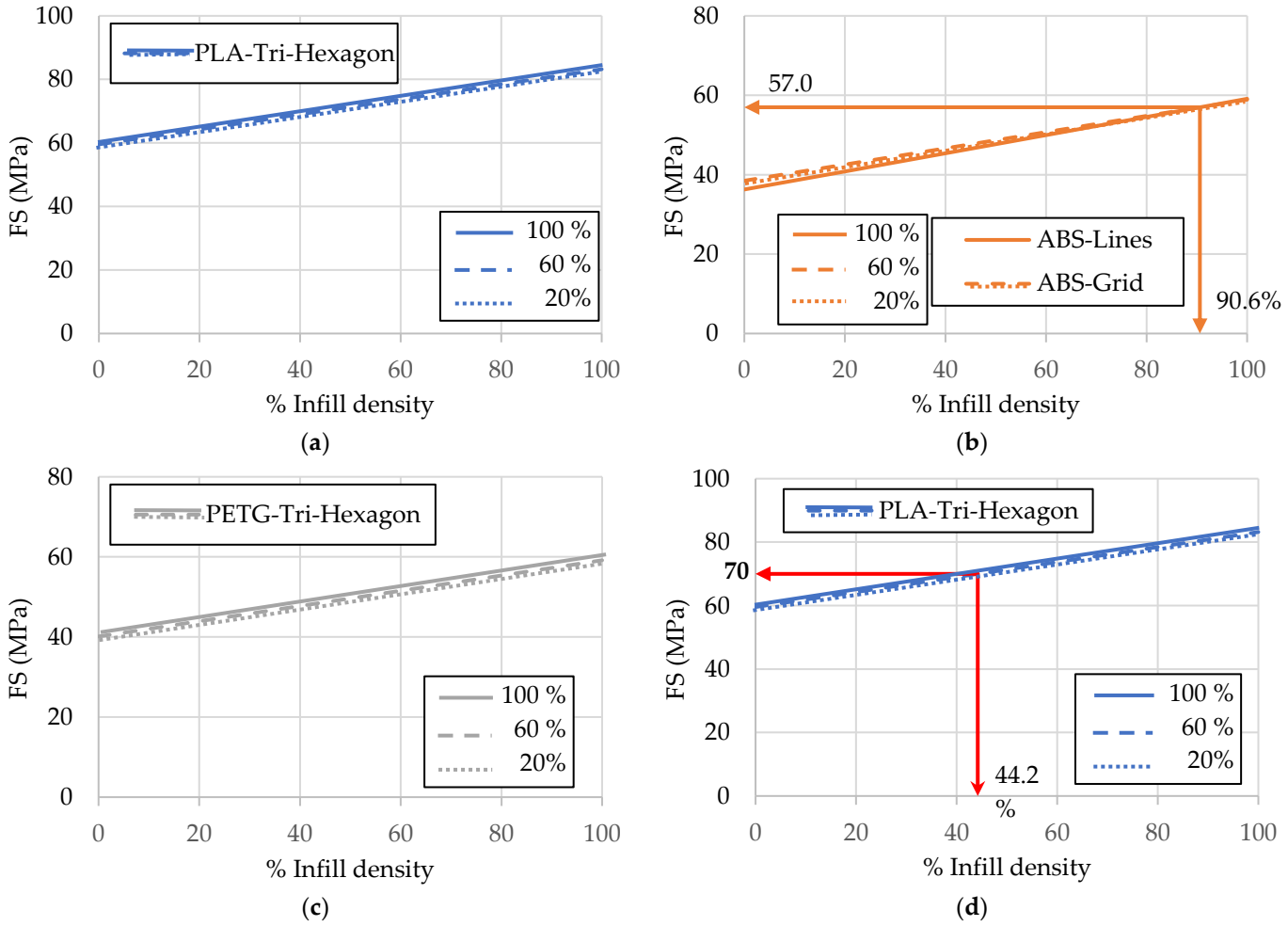


Figure 24. Regression lines for the predicted best-performing patterns for FS as a function of infill density for (**a**) PLA, (**b**) ABS, (**c**) PETG and (**d**) an example for the determination of the best pattern and infill density for a FS target, in this case 70MPa, for the PLA filament.

5.3. Tensile Strength

Figure 25 shows the regression lines for the predicted best-performing patterns for TS as a function of infill density. The intersections indicate the estimated densities at which the predicted best-performing pattern changes. For PLA filament, Figure 25a shows that the cubic pattern exhibited the best performance up to 87.4%; after that, octet was the best one. In the case of ABS (Figure 25b), before 42.4% of infill density, Lines was the best pattern; after that, Cubic was the best. Figure 25c shows that up to an infill density of 38.3%, the Lines pattern exhibited the best performance; between 38.3% and 42.5%, the Cubic pattern was superior, while beyond this point, the Octet pattern showed the best performance for PETG filaments. Figure 25d shows an example for predicting the required infill density to achieve a target tensile strength (e.g., 69.8% infill for 40 MPa) for PLA filaments.

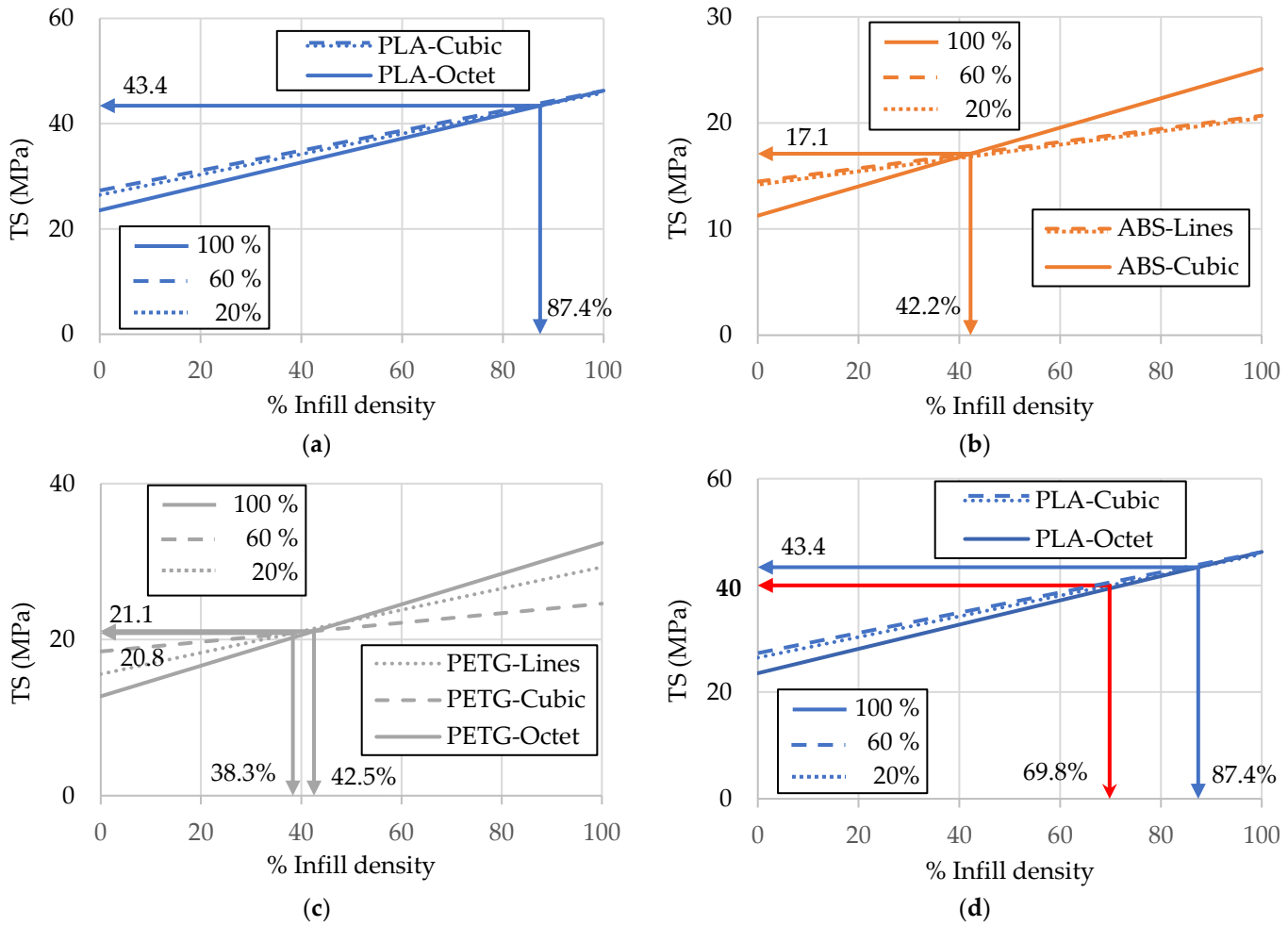


Figure 25. Regression lines for the predicted best-performing patterns for TS as a function of infill density for (**a**) PLA, (**b**) ABS, (**c**) PETG and (**d**) an example for the determination of the best pattern and infill density for a TS target, in this case 40MPa, for the PLA filament.

6. Conclusions

This study provides a comprehensive analysis of how infill density and pattern affect the mechanical behaviour of 3D-printed components made of PLA, ABS, and PETG. Through standardized mechanical testing and statistical analysis, several conclusions can be drawn:

- PLA consistently exhibited superior mechanical strength across all test types: 51.76 MPa in compression, 68.03 MPa in flexure, and 36.60 MPa in tension. These values exceeded those of ABS and PETG by approximately 59–61%, 46–51%, and 73–97%, respectively. Under compression, PETG exhibited the highest mean strain at CS (0.087), compared with 0.061 for PLA and 0.063 for ABS. These comparisons apply to the filament grades and material-specific processing conditions investigated.
- Increasing infill density generally increased strength, as expected. However, no single infill pattern performed best across all conditions. Instead, the most effective pattern varied depending on the filament and the type of mechanical load applied. Tri-Hexagon achieved the highest or statistically equivalent flexural strength for PLA and PETG at all tested densities, whereas Grid performed best for ABS at 20–60% infill and Lines exhibited a slightly higher mean at 100%.
- Hsu's MCB analysis identified the best-performing patterns and those not statistically distinguishable from the best within each investigated condition. The 54 linear regressions described the strength–density relationships, with R^2 values ranging

from approximately 0.70 to 1.00; 44 models yielded $R^2 \geq 0.859$. The equations support preliminary estimates of the density required for a target strength, while intermediate-density estimates and pattern crossover points remain conditional on the assumed linear relationships.

The proposed framework provides preliminary guidance for selecting infill pattern and density according to a specified strength requirement, with potential material savings whose magnitude depends on the complete printing configuration.

Author Contributions: Conceptualization, A.L.-U. and J.V.D.; methodology, A.L.-U. and M.I.L.-M.; software, A.L.-U.; validation, M.I.L.-M.; formal analysis, A.L.-U. and M.I.L.-M.; investigation, A.L.-U. and M.I.L.-M.; resources, R.R.-B. and J.V.D.; data curation, A.L.-U.; writing—original draft preparation, A.L.-U. and M.I.L.-M.; writing—review and editing, A.L.-U., R.R.-B., and M.I.L.-M.; visualization, A.L.-U. and M.I.L.-M.; supervision, R.R.-B. and J.V.D.; project administration, R.R.-B.; funding acquisition, R.R.-B. and J.V.D. All authors have read and agreed to the published version of the manuscript.

Funding: This research received no external funding.

Institutional Review Board Statement: Not applicable.

Data Availability Statement: The data supporting the findings of this study are available from the corresponding author upon reasonable request.

Acknowledgments: This work was supported by the research group TEP 975—Design of (Multifunctional) Materials for Energy Devices—from the University of Córdoba (Spain).

Conflicts of Interest: The authors declare no conflicts of interest.

References

1. Kristiawan, R.B.; Imaduddin, F.; Ariawan, D.; Ubaidillah; Arifin, Z. A Review on the Fused Deposition Modeling (FDM) 3D Printing: Filament Processing, Materials, and Printing Parameters. *Open Eng.* **2021**, *11*, 639–649. https://doi.org/10.1515/eng-2021-0063.
2. Wickramasinghe, S.; Do, T.; Tran, P. FDM-Based 3D Printing of Polymer and Associated Composite: A Review on Mechanical Properties, Defects and Treatments. *Polymers* **2020**, *12*, 1529. https://doi.org/10.3390/POLYM12071529.
3. Kamran, M.; Saxena, A. A Comprehensive Study on 3D Printing Technology. *MIT Int. J. Mech. Eng.* **2016**, *6*, 63–68.
4. Subbarao, C.V.; Reddy, Y.S.; Inturi, V.; Reddy, M.I. Dynamic Mechanical Analysis of 3D Printed PETG Material. *IOP Conf. Ser. Mater. Sci. Eng*. **2021**, *1057*, 012031. https://doi.org/10.1088/1757-899X/1057/1/012031.
5. Riza, M.; Muhida, R.; Efendi, D. Effect of Infill Density on Mechanical Properties of 3D Printed Product for Fused Deposition Modeling Process. *AIP Conf. Proc.* **2023**, *2689*, 070025. https://doi.org/10.1063/5.0114750.
6. Keat, Y.C.; Yin, Y.W.; Ramli, M.Z.; Leng, T.P.; Chie, S.C. Effects of Infill Density on the Mechanical Properties of 3D Printed PLA and Conductive PLA. *AIP Conf. Proc.* **2019**, 2129, 020013. https://doi.org/10.1063/1.5118021.
7. Agrawal, A.P.; Kumar, V.; Kumar, J.; Paramasivam, P.; Dhanasekaran, S.; Prasad, L. An Investigation of Combined Effect of Infill Pattern, Density, and Layer Thickness on Mechanical Properties of 3D Printed ABS by Fused Filament Fabrication. *Heliyon* **2023**, *9*, e16531. https://doi.org/10.1016/J.HELIYON.2023.E16531.
8. Kadhum, A.H.; Al-Zubaidi, S.; Abdulkareem, S.S. Effect of the Infill Patterns on the Mechanical and Surface Characteristics of 3D Printing of PLA, PLA+ and PETG Materials. *ChemEngineering* **2023**, *7*, 46. https://doi.org/10.3390/CHEMENGINEERING7030046.
9. Ortega, N.; Gámez, B.; Ojeda, D.; Erazo, V. Influence of Pattern and Infill Density on the Mechanical Strength of PLA and PETG Parts Printed by FDM. In *Applied Engineering and Innovative Technologies*; Springer: Cham, Switzerland, 2024; pp. 285–293. https://doi.org/10.1007/978-3-031-70760-5_27.
10. Srinivasan, R.; Ruban, W.; Deepanraj, A.; Bhuvanesh, R.; Bhuvanesh, T. Effect on Infill Density on Mechanical Properties of PETG Part Fabricated by Fused Deposition Modelling. *Mater. Today Proc.* **2020**, *27*, 1838–1842. https://doi.org/10.1016/J.MATPR.2020.03.797.

11. Hebda, M.; McIlroy, C.; Whiteside, B.; Caton-Rose, F.; Coates, P. A Method for Predicting Geometric Characteristics of Polymer Deposition during Fused-Filament-Fabrication. *Addit. Manuf.* **2019**, *27*, 99–108. https://doi.org/10.1016/J.ADDMA.2019.02.013.
12. Erdaş, M.U.; Yıldız, B.S.; Yıldız, A.R. Experimental Analysis of the Effects of Different Production Directions on the Mechanical Characteristics of ABS, PLA, and PETG Materials Produced by FDM. *Mater./Mater. Test.* **2024**, *66*, 198–206. https://doi.org/10.1515/mt-2023-0206.
13. Kopar, M.; Yildiz, A.R. Experimental Investigation of Mechanical Properties of PLA, ABS, and PETG 3-d Printing Materials Using Fused Deposition Modeling Technique. *Mater. Test.* **2023**, *65*, 1795–1804. https://doi.org/10.1515/mt-2023-0202.
14. Gao, X.; Qi, S.; Kuang, X.; Su, Y.; Li, J.; Wang, D. Fused Filament Fabrication of Polymer Materials: A Review of Interlayer Bond. *Addit. Manuf.* **2021**, *37*, 101658. https://doi.org/10.1016/J.ADDMA.2020.101658.
15. Xu, S.; Yang, H.; Li, T.; Zhang, Y. Data-Driven Prediction of Mechanical Properties of 3D-Printed Dual-Material Composites Based on Deep Transfer Learning. Compos. *Part A Appl. Sci. Manuf.* **2025**, *198*, 109083. https://doi.org/10.1016/J.COMPOSITESA.2025.109083.
16. Braconnier, D.J.; Jensen, R.E.; Peterson, A.M. Processing Parameter Correlations in Material Extrusion Additive Manufacturing. *Addit. Manuf.* **2020**, *31*, 100924. https://doi.org/10.1016/J.ADDMA.2019.100924.
17. Menargues, S.; Navas, J.; Espinosa, I.; Baile, M.T.; Vaz, R.F.; Picas, J.A. Effect of Additive Manufacturing Parameters on PLA, ABS, and PETG Strength. *Processes* **2025**, *13*, 2733. https://doi.org/10.3390/PR13092733.
18. Kutsal Erhan, I.; Bati, S.; Hisman Celik, Y. Experimental and ANOVA-Based Statistical Analysis of the Effects of Infill Pattern and Density on the Tensile Properties of FDM-Printed ABS, PETG, and PLA Thermoplastics. *Eur. J. Tech.* **2026**, *16*, 32–41. https://doi.org/10.36222/ejt.1833705.
19. Buss, C.; Reci, F.; Hribernig, T.; Steininger, S. Experimental Investigation into the Influence of Infill Density, Print Pattern, and Built-Up Direction on the Flexural Strength of FFF-Manufactured PLA Components. *J. Manuf. Mater. Process.* **2026**, *10*, 21. https://doi.org/10.3390/JMMP10010021.
20. Shehbaz, W.; Peng, Q. Multi-Objective Optimization of FDM Infill Patterns Using Design of Experiments Considering Load-Path Alignment. *Eng* **2026**, *7*, 175. https://doi.org/10.3390/ENG7040175.
21. UNE-EN ISO 604:2003; *Plastics—Determination of Compressive Properties (ISO 604:2002)*, corrected version, November 2021. Asociación Española de Normalización (UNE): Madrid, Spain, 2003.
22. UNE-EN ISO 178:2020; *Plastics—Determination of Flexural Properties (ISO 178:2019)*. Asociación Española de Normalización (UNE): Madrid, Spain, 2020.
23. UNE-EN ISO 527-1:2020; *Plastics—Determination of Tensile Properties—Part 1: General Principles (ISO 527-1:2019)*. Asociación Española de Normalización (UNE): Madrid, Spain, 2020.
24. UNE-EN ISO 20753:2019; *Plastics—Test Specimens (ISO 20753:2018)*. Asociación Española de Normalización (UNE): Madrid, Spain, 2019.
25. Hsueh, M.H.; Lai, C.J.; Wang, S.H.; Zeng, Y.S.; Hsieh, C.H.; Pan, C.Y.; Huang, W.C. Effect of printing parameters on the thermal and mechanical properties of 3d-printed pla and petg, using fused deposition modeling. *Polymers* **2021**, *13*, 1758. https://doi.org/10.3390/polym13111758.
26. D'andrea, D.; Risitano, G.; Raffaele, M.; Cucinotta, F.; Santonocito, D. Damage Assessment of Different FDM-Processed Materials Adopting Infrared Thermography. *Frat. Integrita Strutt.* **2022**, *16*, 75–90. https://doi.org/10.3221/IGF-ESIS.62.06.
27. Algarni, M.; Ghazali, S. Comparative Study of the Sensitivity of PLA, ABS, PEEK, and PETG's Mechanical Properties to FDM Printing Process Parameters. *Crystals* **2021**, *11*, 995. https://doi.org/10.3390/CRYST11080995.
28. Edwards, D.G.; Hsu, J.C. Multiple Comparisons with the Best Treatment. *J. Am. Stat. Assoc.* **1983**, *78*, 965–971. https://doi.org/10.1080/01621459.1983.10477047.
29. Daly, M.; Tarfaoui, M.; Bouali, M.; Bendarma, A. Effects of Infill Density and Pattern on the Tensile Mechanical Behavior of 3D-Printed Glycolyzed Polyethylene Terephthalate Reinforced with Carbon-Fiber Composites by the FDM Process. *J. Compos. Sci.* **2024**, *8*, 115. https://doi.org/10.3390/JCS8040115.

Disclaimer/Publisher's Note: The statements, opinions and data contained in all publications are solely those of the individual author(s) and contributor(s) and not of MDPI and/or the editor(s). MDPI and/or the editor(s) disclaim responsibility for any injury to people or property resulting from any ideas, methods, instructions or products referred to in the content.